IOP PUBLISHING PHYSICS IN MEDICINE AND BIOLOGY

Phys. Med. Biol. **54** (2009) 67–90 doi:10.1088/0031-9155/54/1/005

A higher order diffusion model for three-dimensional photon migration and image reconstruction in optical tomography

Zhen Yuan[1], **Xin-Hua Hu**[2] **and Huabei Jiang**[1]

[1] Department of Biomedical Engineering, University of Florida, Gainesville, FL 32611, USA
[2] Department of Physics, East Carolina University, Greenville, NC 27858, USA

E-mail: hjiang@bme.ufl.edu

Received 10 July 2008, in final form 29 October 2008
Published 5 December 2008
Online at stacks.iop.org/PMB/54/67

Abstract

In this work, we derived three-dimensional simplified spherical harmonics approximated higher order diffusion equations. We also solved the higher order diffusion equations using a finite element method and compared the solutions from the first-order diffusion equation and Monte Carlo simulations. We found that the conducted model is able to improve the first-order diffusion solution in a transport-like homogeneous or heterogeneous medium. Reconstructed images based on the higher order diffusion model are also presented. We conclude that the developed higher order diffusion model is able to accurately describe light propagation in biological tissues and to offer improved image reconstruction.

(Some figures in this article are in colour only in the electronic version)

1. Introduction

The development of a model to describe light migration in turbid media is essential for the assessment of measurements in diagnostic near-infrared spectroscopy and imaging optical properties of biological tissues (Yodh and Chance 1995, Boas 1995, Barbour *et al* 1993, Hebden *et al* 1997, Dehghani *et al* 1999, Jiang *et al* 1996, Boverman *et al* 2007, Unlu *et al* 2008, Kanmani and Vasu 2007). Current modeling of light propagation in scattering tissues is largely through the utilization of the first-order diffusion approximation to the radiation transport equation. However, the first-order diffusion approximation is not very accurate to simulate photon transport in some particular regions including low-scattering or high-absorption tissues with clear fluids, clear layers with low scattering and low absorption or turbid media with highly heterogeneous optical properties. In particular, it is very challenging for the diffusion approximation to describe the photon migration in small-volume tissues, such as arthritis in finger joints and body parts in small animals due to the small optical distance between sources and detectors (Hielscher *et al* 1998). Limitation of the first-order diffusion

approximation has been investigated extensively and some endeavors have also been made to improve the model (Dehghani *et al* 1999, Kim *et al* 1998, Elaloufi *et al* 2003).

The equation of radiation transport (RTE) has been addressed as an accurate model to describe light migration in scattering media. However, the RTE is difficult to solve, even in homogeneous media with simple boundaries. Additionally, solving the inverse problem for optical tomography with RTE is an even more daunting and time-consuming task. Instead, several approximations to the RTE including the discrete ordinates (s_n) and spherical harmonics (p_n) equations have been presented to overcome the limitations for directly solving the RTE. For example, a time-independent, finite-difference, s_n-based three-dimensional (3D) transport model has been employed by Hielscher to calculate photon migration in biological tissues or to image small-volume tissues (Hielscher *et al* 1998, Klose *et al* 2002, Rui *et al* 2007). However, the forward solution and reconstruction computation based on this model is time consuming. Typically, the reconstruction algorithm based on the s_n approximated transport model is 40–60 times slower than that from the diffusion approximation (Rui *et al* 2007).

An alternative to the s_n method is the p_n approach that has the advantage of expressing the angular dependence of the specific intensity in a basis of analytical functions rather than in the completely local basis of discrete ordinates. Additionally, the p_n methodology is based on a variational formulation for the second-order form of the transport equation and it is the most natural and numerically efficient way of deriving higher order diffusion approximations. Unfortunately, most of the developed higher order diffusion approximated transport models based on the p_n method for describing light migration in biological tissues are only limited for two-dimensional (2D) cases (Aydin *et al* 2002, 2004, Xu *et al* 2001, Dorn 1998, Jiang 1999, Kim and Ishimaru 1998, Aronson and Corngold 1999).

In this study, we attempt to derive a 3D simplified p_3 approximated RTE (third-order diffusion equation) from the Boltzmann transport equation without the assumptions that are applied to the first-order diffusion approximation. We use a finite element (FE) method to solve the developed equations for photon transport in some typical media with particular optical properties. After comparing the results with those from the first-order diffusion equation and Monte Carlo (MC) simulations, we found that the developed equations are able to provide solutions that are significantly more accurate than the first-order diffusion equation and the solutions also agree well with MC simulations (Song *et al* 1999). Moreover, the reconstruction algorithm based on the developed higher order diffusion equations is not computationally demanding due to the utilization of simplified p_3 approximation. Initial estimation indicates that the first-order diffusion approximation-based reconstruction algorithm is only 1.5–2.0 times faster than the higher order diffusion equations-based algorithm when a finite element mesh of 3009 nodes and 64 sources and 64 detectors are used. We note that the higher order diffusion equations-based algorithm has the advantage of using the same economic, portable optical measurement systems as the first-order diffusion approximation-based algorithm. In addition, the hyperbolic-type higher order diffusion equations are able to provide more stable inverse solutions than the parabolic-type first-order diffusion equation. Using imaging in the finger joints as an example (Yuan *et al* 2007, 2008), we observed significant differences between the reconstructed results from the first-order and higher order diffusion equations. We also found that errors for the recovered optical properties of small-volume tissues do exist using the first-order diffusion approximation-based algorithm.

2. Theoretical background

When a continuous-wave light source is used, the migration of photons within the absorbing and scattering media can be described by the time- and energy-independent form of Boltzmann

transport equation as

$$\Omega \cdot \nabla \Phi(r, \Omega) + \sigma_t(r)\Phi(r, \Omega) = \int \sigma_s(\Omega', \Omega, r)\Phi(r, \Omega')\, \mathrm{d}\Omega' + s(r, \Omega) \tag{1}$$

where r is the position vector of a photon propagation along the direction by the unit direction Ω, $\Phi(r, \Omega)$ is the energy radiance, $s(r\ \Omega)$ is the source term, $\sigma_t(r)$ is the total position-dependent macroscopic transport cross section (absorption + scattering) and $\sigma_s(r, \Omega' - \Omega)$ is the differential macroscopic scattering cross section. The radiance using spherical harmonics at position r in the direction of unit vector Ω can be expanded as a series of the form

$$\Phi(r, \Omega) = \sum_{l=0}^{N} \sum_{m=0}^{l} (2l+1)\, p_l^m(\cos\theta)\, [\psi_{lm}(r)\cos(m\phi) + \gamma_{lm}(r)\sin(m\phi)] \tag{2}$$

where $p_l^m(\cos\theta)$ are associated Legendre polynomials of order l, m; $\psi_{lm}(r)$, $\gamma_{lm}(r)$ are the coefficients of moments of the series; and θ and ϕ are the axial and azimuthal angles respectively of Ω. In consideration of the gradient operator for the 3D case

$$\Omega \cdot \nabla = \cos\theta \frac{\partial}{\partial z} + \sin\theta\cos\phi \frac{\partial}{\partial x} + \sin\theta\sin\phi \frac{\partial}{\partial y},$$

equation (1) can be written as the following when one substitutes equation (2) into equation (1):

$$\begin{aligned}
&\sum_{l=0}^{N}\sum_{m=0}^{l} (2l+1)\, p_l^m \cos\theta \left(\cos m\phi \frac{\partial \psi_{lm}}{\partial z} + \sin m\phi \frac{\partial \gamma_{lm}}{\partial z}\right) \\
&\quad + \sum_{l=0}^{N}\sum_{m=0}^{l} (2l+1)\, p_l^m \sin\theta\sin\phi \left(\cos m\phi \frac{\partial \psi_{lm}}{\partial y} + \sin m\phi \frac{\partial \gamma_{lm}}{\partial y}\right) \\
&\quad + \sum_{l=0}^{N}\sum_{m=0}^{l} (2l+1)\, p_l^m \sin\theta\cos\phi \left(\cos m\phi \frac{\partial \psi_{lm}}{\partial x} + \sin m\phi \frac{\partial \gamma_{lm}}{\partial x}\right) \\
&\quad + \sigma_t \sum_{l=0}^{N}\sum_{m=0}^{l} (2l+1)\, p_l^m (\cos m\phi\, \psi_{lm} + \sin m\phi\, \gamma_{lm}) \\
&\quad + \int \sigma_s(\cos\Theta, r) \sum_{l'=0}^{N}\sum_{m'=0}^{l'} (2l'+1)\, p_{l'}^{m'} \\
&\quad \times (\cos m'\phi'\psi_{l'm'} + \sin m'\phi'\gamma_{l'm'})\, \mathrm{d}\Omega' = s(r, \Omega)
\end{aligned} \tag{3}$$

where $\cos\Theta \equiv \Omega \cdot \Omega'$. When the ϕ products are expanded, the second term in equation (3) is given by

$$\begin{aligned}
&\sum_{l}\sum_{m} (2l+1)\, p_l^m \sin\theta \left[\frac{1}{2}(\sin(m+1)\phi - \sin(m-1)\phi)\frac{\partial \psi_{lm}}{\partial y}\right. \\
&\quad \left. + \frac{1}{2}(-\cos(m+1)\phi + \cos(m-1)\phi)\frac{\partial \gamma_{lm}}{\partial y}\right],
\end{aligned} \tag{4}$$

and the third term in equation (3) is written as

$$\begin{aligned}
&\sum_{l}\sum_{m} (2l+1)\, p_l^m \sin\theta \left[\frac{1}{2}(\cos(m+1)\phi + \cos(m-1)\phi)\frac{\partial \psi_{lm}}{\partial x}\right. \\
&\quad \left. + \frac{1}{2}(\sin(m+1)\phi + \sin(m-1)\phi)\frac{\partial \gamma_{lm}}{\partial x}\right].
\end{aligned} \tag{5}$$

Moreover, the last term in equation (3) is further written as

$$\int \sigma_s(\cos\Theta, r)\sum_{l'=0}^{N}\sum_{m'=0}^{l'}(2l'+1)p_{l'}^{m'}(\cos m'\phi'\psi_{l'm'}+\sin m'\phi'\gamma_{l'm'})\,\mathrm{d}\Omega',$$

$$=\int\sum_{l}\sigma_l(r)p_l(\cos\Theta)\sum_{l'=0}^{N'}\sum_{m'=0}^{l'}(2l'+1)p_{l'}^{m'}(\cos m'\phi'\psi_{l'm'}+\sin m'\phi'\gamma_{l'm'})\,\mathrm{d}\Omega'$$

$$=\int\sum_{l=0}^{N}\sigma_l\left\{p_l(\cos\theta)p_l+2\sum_{m=1}^{l}\frac{(l-m)!}{(l+m)!}p_l^m(\cos\theta)p_l^m(\cos\theta')\cos[m(\varphi-\varphi')]\right\}$$

$$\times\sum_{l'=0}^{N'}\sum_{m'=0}^{l'}(2l'+1)p_{l'}^{m'}(\cos m'\phi'\psi_{l'm'}+\sin m'\phi'\gamma_{l'm'})\,\mathrm{d}\Omega'. \tag{6a}$$

According to Whittaker and Watson modern analysis (Oak Ridge National Laboratory Report 1990), the phase function term in equation (6*a*) can be absorbed into the transport cross section giving a term

$$\sum\sigma_{lm}(2l+1)p_l^m(\psi_{ml}\cos m\phi+\gamma_{ml}\sin m\phi). \tag{6b}$$

After substitution of equations (4)–(6) into the photon transport equation (3), we get

$$\sum_{l=0}^{N}\sum_{m=0}^{l}(2l+1)p_l^m\cos\theta\left(\cos m\phi\frac{\partial\psi_{lm}}{\partial z}+\sin m\phi\frac{\partial\gamma_{lm}}{\partial z}\right)$$

$$+\sum\sigma_{lm}(2l+1)p_l^m(\psi_{ml}\cos m\phi+\gamma_{ml}\sin m\phi)\sum_{l}\sum_{m}(2l+1)p_l^m\sin\theta$$

$$\times\left[\frac{\cos(m+1)\phi}{2}\left(\frac{\partial\psi_{lm}}{\partial x}-\frac{\partial\gamma_{lm}}{\partial y}\right)+\frac{\cos(m-1)\phi}{2}\left(\frac{\partial\psi_{lm}}{\partial x}+\frac{\partial\gamma_{lm}}{\partial y}\right)\right]$$

$$+\sum_{l}\sum_{m}(2l+1)p_l^m\sin\theta\left[\frac{\sin(m+1)\phi}{2}\left(\frac{\partial\psi_{lm}}{\partial y}+\frac{\partial\gamma_{lm}}{\partial x}\right)\right.$$

$$\left.+\frac{\sin(m-1)\phi}{2}\left(-\frac{\partial\psi_{lm}}{\partial y}+\frac{\partial\gamma_{lm}}{\partial x}\right)\right]=s(r,\Omega). \tag{7}$$

With the following recurrence

$$(2l+1)\cos\theta p_l^m=(l-m+1)p_{l+1}^m+(l+m)p_{l-1}^m \tag{8a}$$

$$(2l+1)\sin\theta p_l^m=p_{l+1}^{m+1}-p_{l-1}^{m+1} \tag{8b}$$

$$(2l+1)\sin\theta p_l^m=(l+m)(l+m-1)\times p_{l-1}^{m-1}-(l-m+1)\times(l-m+2)p_{l+1}^{m-1} \tag{8c}$$

equation (7) is further written as

$$\sum_{l}\sum_{m}\left[(l-m+1)p_{l+1}^m+(l+m)p_{l-1}^m\right]\left(\cos m\phi\frac{\partial\psi_{lm}}{\partial z}+\sin m\phi\frac{\partial\gamma_{lm}}{\partial z}\right)$$

$$+\sum\sigma_{lm}(2l+1)p_l^m(\psi_{ml}\cos m\phi+\gamma_{ml}\sin m\phi)+\sum_{l}\sum_{m}\left[p_{l+1}^{m+1}-p_{l-1}^{m+1}\right]$$

$$\times\left[\frac{\cos(m+1)\phi}{2}\left(\frac{\partial\psi_{lm}}{\partial x}-\frac{\partial\gamma_{lm}}{\partial y}\right)+\frac{\sin(m+1)\phi}{2}\left(\frac{\partial\psi_{lm}}{\partial y}+\frac{\partial\gamma_{lm}}{\partial x}\right)\right]$$

$$+\sum_{l}\sum_{m}\left[(l+m)(l+m-1)p_{l-1}^{m-1}-(l-m+1)(l-m+2)p_{l+1}^{m-1}\right]$$

$$\times\left[\frac{\cos(m-1)\phi}{2}\left(\frac{\partial\psi_{lm}}{\partial x}+\frac{\partial\gamma_{lm}}{\partial y}\right)\right.$$
$$\left.+\frac{\sin(m-1)\phi}{2}\left(-\frac{\partial\psi_{lm}}{\partial y}+\frac{\partial\gamma_{lm}}{\partial x}\right)\right]=s(r,\Omega). \tag{9}$$

Compare $p_l^m\cos m\phi$,

$$2(l-m)\frac{\partial\psi_{l-1,m}}{\partial z}+2(l+m+1)\frac{\partial\psi_{l+1,m}}{\partial z}+\left(\frac{\partial\psi_{l-1,m-1}}{\partial x}-\frac{\partial\gamma_{l-1,m-1}}{\partial y}\right)$$
$$-\left(\frac{\partial\psi_{l+1,m-1}}{\partial x}-\frac{\partial\gamma_{l+1,m-1}}{\partial y}\right)+(l+m+2)(l+m+1)\left(\frac{\partial\psi_{l+1,m+1}}{\partial x}+\frac{\partial\gamma_{l+1,m+1}}{\partial y}\right)$$
$$-(l-m-1)(l-m)\left(\frac{\partial\psi_{l-1,m+1}}{\partial x}+\frac{\partial\gamma_{l-1,m+1}}{\partial y}\right)+2(2l+1)\sigma_{lm}\psi_{lm}=s\delta_l^0. \tag{10}$$

Compare $p_l^m\sin m\phi$,

$$2(l-m)\frac{\partial\gamma_{l-1,m}}{\partial z}+2(l+m+1)\frac{\partial\gamma_{l+1,m}}{\partial z}+\left(\frac{\partial\psi_{l-1,m-1}}{\partial y}+\frac{\partial\gamma_{l-1,m-1}}{\partial x}\right)$$
$$-\left(\frac{\partial\psi_{l+1,m-1}}{\partial y}+\frac{\partial\gamma_{l+1,m-1}}{\partial x}\right)+(l+m+2)(l+m+1)$$
$$\times\left(-\frac{\partial\psi_{l+1,m+1}}{\partial y}+\frac{\partial\gamma_{l+1,m+1}}{\partial x}\right)-(l-m-1)(l-m)$$
$$\times\left(-\frac{\partial\psi_{l-1,m+1}}{\partial y}+\frac{\partial\gamma_{l-1,m+1}}{\partial x}\right)+2(2l+1)\sigma_{lm}\gamma_{lm}=0. \tag{11}$$

Equations (10) and (11) are the derived 3D p_n approximated radiation transport equations. The approximations of p_3, p_5 and p_7 have been performed in various geometries for 2D problems and the results validating the p_3 calculation are sufficiently accurate (Aydin *et al* 2002, Klose *et al* 2002). As such, a serial of moment equations based on the p_3 approximation are derived for 3D cases to reduce the computational cost with accepted numerical accuracy. As a consequence, six p_3 approximated multiple-group transport equations are derived with six variables (ψ_{00}, ψ_{20}, ψ_{22}, ψ_{21}, γ_{21}, γ_{22}) if we assume σ_{lm} are equal except for σ_{11} (see the appendix):

$$\frac{2}{3}\left(\frac{\partial^2\psi_{00}}{\partial^2x}+\frac{\partial^2\psi_{00}}{\partial^2y}+\frac{\partial^2\psi_{00}}{\partial^2z}\right)+\left(\frac{4}{3}\frac{\partial^2\psi_{20}}{\partial^2z}-\frac{2}{3}\frac{\partial^2\psi_{20}}{\partial^2x}-\frac{2}{3}\frac{\partial^2\psi_{20}}{\partial^2y}\right)+4\left(\frac{\partial^2\psi_{22}}{\partial^2x}\right)$$
$$+4\frac{\partial^2\psi_{21}}{\partial z\partial x}+4\frac{\partial^2\gamma_{21}}{\partial z\partial y}+4\left(-\frac{\partial^2\psi_{22}}{\partial^2y}\right)+8\frac{\partial^2\gamma_{22}}{\partial x\partial y}-2\sigma_{00}\sigma_{11}\psi_{00}=-S_1 \tag{12}$$

$$\frac{50}{21}\left(\frac{\partial^2\psi_{20}}{\partial^2x}+\frac{\partial^2\psi_{20}}{\partial^2y}\right)+\frac{4}{3}\left(\frac{\partial^2\psi_{00}}{\partial^2z}-\frac{1}{2}\frac{\partial\psi_{00}^2}{\partial^2x}-\frac{1}{2}\frac{\partial\psi_{00}^2}{\partial^2y}\right)+\frac{40}{7}\left(\frac{\partial^2\psi_{22}}{\partial^2y}-\frac{\partial^2\psi_{22}}{\partial x}-2\frac{\partial^2\gamma_{22}}{\partial x\partial y}\right)$$
$$+\frac{110}{21}\frac{\partial^2\psi_{20}}{\partial^2z}+\frac{20}{7}\left(\frac{\partial^2\psi_{21}}{\partial z\partial x}+\frac{\partial^2\gamma_{21}}{\partial z\partial y}\right)-10\sigma_{00}^2\psi_{20}=0 \tag{13}$$

$$\frac{1}{3}\left(\frac{\partial^2\psi_{00}}{\partial^2x}-\frac{\partial^2\psi_{00}}{\partial^2y}\right)-\frac{10}{21}\left(\frac{\partial^2\psi_{20}}{\partial^2x}-\frac{\partial^2\psi_{20}}{\partial^2y}\right)+\frac{10}{7}\left(\frac{\partial^2\psi_{21}}{\partial x\partial z}-\frac{\partial^2\gamma_{21}}{\partial y\partial z}\right)$$
$$+\frac{30}{7}\left(\frac{\partial\psi_{22}^2}{\partial^2x}+\frac{\partial\psi_{22}^2}{\partial^2y}+\frac{1}{3}\frac{\partial^2\psi_{22}}{\partial^2z}\right)-10\sigma_{00}^2\psi_{22}=0 \tag{14}$$

$$\frac{2}{3}\frac{\partial^2\psi_{00}}{\partial x\partial y}-\frac{20}{21}\frac{\partial^2\psi_{20}}{\partial x\partial y}+\frac{30}{7}\left(\frac{\partial\gamma_{22}^2}{\partial^2 x}+\frac{\partial\gamma_{22}^2}{\partial^2 y}+\frac{1}{3}\frac{\partial^2\gamma_{22}}{\partial^2 z}\right)$$
$$+\frac{10}{7}\left(\frac{\partial^2\psi_{21}}{\partial y\partial z}+\frac{\partial\gamma_{21}^2}{\partial x\partial z}\right)-10\sigma_{00}^2\gamma_{22}=0 \tag{15}$$

$$\frac{4}{3}\frac{\partial^2\psi_{00}}{\partial x\partial z}+\frac{20}{21}\frac{\partial^2\psi_{20}}{\partial x\partial z}+\frac{30}{7}\left(\frac{\partial^2\psi_{21}}{\partial^2 z}+\frac{\partial^2\psi_{21}}{\partial^2 x}+\frac{1}{3}\frac{\psi^2{}_{21}}{\partial^2 y}\right)$$
$$+\frac{40}{7}\left(\frac{\partial^2\psi_{22}}{\partial x\partial z}+\frac{\partial\gamma^2{}_{22}}{\partial y\partial z}+\frac{1}{2}\frac{\partial^2\gamma_{21}}{\partial z\partial y}\right)-10\sigma_{00}^2\psi_{21}=0 \tag{16}$$

$$\frac{4}{3}\frac{\partial^2\psi_{00}}{\partial y\partial z}+\frac{20}{21}\frac{\partial^2\psi_{20}}{\partial y\partial z}+\frac{30}{7}\left(\frac{\partial^2\gamma_{21}}{\partial^2 z}+\frac{1}{3}\frac{\partial^2\gamma_{21}}{\partial^2 x}+\frac{\gamma_{21}^2}{\partial^2 y}\right)$$
$$+\frac{40}{7}\left(\frac{\partial^2\gamma_{22}}{\partial x\partial z}-\frac{\partial\psi_{22}^2}{\partial y\partial z}+\frac{1}{2}\frac{\partial^2\psi_{21}}{\partial x\partial y}\right)-10\sigma_{00}^2\gamma_{21}=0. \tag{17}$$

If we specify $\sigma_{lm}=\mu_t'=\mu_a+\mu_s$ except for $\sigma_{11}=\mu_a$ and the diffusion coefficient $D=1/3\mu_t'$, the multiple-group transport equations are further written as

$$D\left(\frac{\partial^2\psi_1}{\partial^2 x}+\frac{\partial^2\psi_1}{\partial^2 y}+\frac{\partial^2\psi_1}{\partial^2 z}\right)-\mu_a\psi_1+D\left(2\frac{\partial^2\psi_2}{\partial^2 z}-\frac{\partial^2\psi_2}{\partial^2 x}-\frac{\partial^2\psi_2}{\partial^2 y}\right)+6D\left(\frac{\partial^2\psi_3}{\partial^2 x}\right)$$
$$+6D\left(-\frac{\partial^2\psi_3}{\partial^2 y}\right)+6D\frac{\partial^2\psi_5}{\partial z\partial x}+6D\frac{\partial^2\psi_6}{\partial z\partial y}+6D\frac{\partial^2\psi_4}{\partial x\partial y}+6D\frac{\partial^2\psi_4}{\partial y\partial x}=-S(r) \tag{18}$$

$$\frac{25}{7}D\left(\frac{\partial^2\psi_2}{\partial^2 x}+\frac{\partial^2\psi_2}{\partial^2 y}\right)+2D\left(\frac{\partial^2\psi_1}{\partial^2 z}-\frac{1}{2}\frac{\partial^2\psi_1}{\partial^2 x}-\frac{1}{2}\frac{\partial^2\psi_1}{\partial^2 y}\right)$$
$$+\frac{60}{7}D\left(\frac{\partial^2\psi_3}{\partial^2 y}-\frac{\partial^2\psi_3}{\partial^2 x}-\frac{\partial^2\psi_4}{\partial x\partial y}-\frac{\partial^2\psi_4}{\partial y\partial x}\right)$$
$$+\frac{55}{7}D\frac{\partial^2\psi_2}{\partial^2 z}+\frac{30}{7}D\left(\frac{\partial^2\psi_5}{\partial z\partial x}+\frac{\partial^2\psi_6}{\partial z\partial y}\right)-5\mu_t'\psi_2=0 \tag{19}$$

$$D\left(\frac{\partial^2\psi_1}{\partial^2 x}-\frac{\partial^2\psi_1}{\partial^2 y}\right)-\frac{10}{7}D\left(\frac{\partial^2\psi_2}{\partial^2 x}-\frac{\partial^2\psi_2}{\partial^2 y}\right)+\frac{30}{7}D\left(\frac{\partial^2\psi_5}{\partial x\partial z}-\frac{\partial^2\psi_6}{\partial y\partial z}\right)$$
$$+\frac{90}{7}D\left(\frac{\partial^2\psi_3}{\partial^2 x}+\frac{\partial^2\psi_3}{\partial^2 y}+\frac{1}{3}\frac{\partial^2\psi_3}{\partial^2 z}\right)-10\mu_t'\psi_3=0 \tag{20}$$

$$\frac{1}{2}D\frac{\partial^2\psi_1}{\partial x\partial y}+\frac{1}{2}D\frac{\partial^2\psi_1}{\partial y\partial x}-\frac{5}{7}D\frac{\partial^2\psi_2}{\partial x\partial y}-\frac{5}{7}D\frac{\partial^2\psi_2}{\partial y\partial x}+\frac{45}{7}D\left(\frac{\partial^2\psi_4}{\partial^2 x}+\frac{\partial^2\psi_4}{\partial^2 y}+\frac{1}{3}\frac{\partial^2\psi_4}{\partial^2 z}\right)$$
$$+\frac{15}{7}D\left(\frac{\partial^2\psi_5}{\partial y\partial z}+\frac{\partial^2\psi_6}{\partial x\partial z}\right)-5\mu_t'\psi_4=0 \tag{21}$$

$$2D\frac{\partial^2\psi_1}{\partial x\partial z}+\frac{10}{7}D\frac{\partial^2\psi_2}{\partial x\partial z}+\frac{45}{7}D\left(\frac{\partial^2\psi_5}{\partial^2 z}+\frac{\partial^2\psi_5}{\partial^2 x}+\frac{1}{3}\frac{\partial^2\psi_5}{\partial^2 y}\right)$$
$$+\frac{60}{7}D\left(\frac{\partial^2\psi_3}{\partial x\partial z}+\frac{\partial^2\psi_4}{\partial y\partial z}+\frac{1}{2}\frac{\partial^2\psi_6}{\partial z\partial y}\right)-5\mu_t'\psi_5=0 \tag{22}$$

$$2D\frac{\partial^2\psi_1}{\partial y\partial z}+\frac{10}{7}D\frac{\partial^2\psi_2}{\partial y\partial z}+\frac{45}{7}D\left(\frac{\partial^2\psi_6}{\partial^2 z}+\frac{1}{3}\frac{\partial^2\psi_6}{\partial^2 x}+\frac{\partial^2\psi_6}{\partial^2 y}\right)$$
$$+\frac{60}{7}D\left(\frac{\partial^2\psi_4}{\partial x\partial z}-\frac{\partial^2\psi_3}{\partial y\partial z}+\frac{1}{2}\frac{\partial^2\psi_5}{\partial x\partial y}\right)-5\mu_t'\psi_6=0. \tag{23}$$

It is noted from equations (3)–(6) that the phase function is automatically absorbed into the transport cross-section term. As a consequence, the total position-dependent macroscopic transport cross-section coefficient μ_t' (absorption + scattering) should encompass the effect of anisotropical scattering coefficient. In addition, for consistency, the diffusion coefficient D in equations (18)–(23) is further simplified while $\mu_t'=\mu_a+\mu_s$ is invariable:

$$D=1/(3\mu_a+3\mu_s(1-g)) \tag{24}$$

where μ_a is the absorption coefficient, μ_s is the scattering coefficient and g is the scattering anisotropic factor (note that the reduced scattering coefficient $\mu_s'=(1-g)\mu_s$). We name equations (18)–(23) the 3D p_3 approximated higher order diffusion equations. It should be pointed out they can be further reduced to the first-order diffusion equation by setting $\psi_2=\psi_3=\psi_4=\psi_5=\psi_6=0$:

$$\nabla\cdot D(r)\nabla\psi(r)-\mu_a(r)\psi(r)=-S(r). \tag{25}$$

Appropriate boundary conditions (BCs) should be specified for the higher order diffusion equations. In this study, type III BCs are used for the first component ψ_1 while type I BCs are assumed for the other five components:

$$-D\nabla\psi_1\cdot n=\alpha\psi_1,\ \ \psi_2=\psi_3=\psi_4=\psi_5=\psi_6=0. \tag{26}$$

Type III BCs are generally applied in diffuse optical imaging field and contains the linear combination of the photon density and the current at $\partial\Omega$ (α is the BC coefficient and $\alpha=0.467$ for the vacuum case) while the type I BCs are the commonly used approximate BCs for the RTE model. As such, the utilized mixed BCs can be easily extended to formulate the FE solution equations for the developed model with high numerical accuracy. In addition, they are able to reduce the computational cost greatly due to a great mount of enforced zero variables. To solve the multi-group transport equations by the FE method, the parameters $\psi(r)$, μ_t', D and μ_a are spatially discretized as

$$\psi_k=\sum_{i=1}^{N}L_i(\psi_k)_i,\qquad \mu_t'=\sum_{i=1}^{N}L(i)\mu_t',\qquad D=\sum_{i=1}^{N}D_iL_i,\qquad \mu_a=\sum_{i=1}^{N}(\mu_a)_iL_i \tag{27}$$

where N is the node number of the 3D FE mesh and L_i is the basis function.

As such, the discretized form of equations (18)–(23) and (26) can be written as

$$[A]\{\psi\}=\{b\} \tag{28}$$

where the elements of the matrix $[A]$ are integrated over the problem domain (V) and boundary domain (Γ), and $\{b\}$ is the source vector. The inverse solution is obtained through the following equations:

$$[A]\{\partial\psi/\partial\chi\}=\{\partial b/\partial\chi\}-[\partial A/\partial\chi]\{\psi\} \tag{29}$$
$$(\Im^T\Im+\lambda\mathbf{I})\Delta\boldsymbol{\chi}=\Im^T(\boldsymbol{\psi}^o-\boldsymbol{\psi}^c) \tag{30}$$

where $\boldsymbol{\chi}$ expresses D or μ_a, and $\Im$ is the Jacobian matrix formed by $\partial\psi/\partial\chi$ at the boundary measurement sites. λ, a regularization scalar, and $\boldsymbol{I}$, the identity matrix, are used to realize

the stable inversion of equation (30). $\Delta\boldsymbol{\chi} = (\Delta D_1, \Delta D_2, \ldots, \Delta D_N, \Delta\mu_{a,1}, \Delta\mu_{a,2}, \ldots, \Delta\mu_{a,N})^T$. $\boldsymbol{\psi}^o = \left(\psi_1^{1o}, \psi_1^{2o}, \ldots, \psi_1^{Mo}\right)^T$ and $\boldsymbol{\psi}^c = \left(\psi_1^{1c}, \psi_1^{2c}, \ldots, \psi_1^{Mc}\right)^T$, where ψ_1^o and ψ_1^c are observed and computed photon density (the first component) for $i = 1, 2, \ldots, M$ boundary locations. It should be noted that only the first component is utilized for inverse computation due to the fact that the other five moment variables are equal to zero at the boundary measurement positions. Thus the image formation task here is to update optical property distributions via iterative solution of equations (28) and (30) so that a weighted sum of the squared difference between computed and measured photon density can be minimized.

3. Results

In the remainder of this part, we first demonstrate the results calculated using first-order and higher order diffusion equations for photon propagation inside a small-volume tissue, in which the effect of the ratio of absorption to scattering coefficient on the accuracy of first-order diffusion approximation is quantified. We then discuss in detail the effect of non-scattering, void-like regions on the photon propagation through a 3D medium. Further, the computed results obtained from the higher order diffusion model are compared with those from MC simulations and diffusion approximation. Finally, we perform image reconstructions using two models that mimic imaging in the finger joints, and the recovered images from the two models are presented herein.

3.1. Homogeneous medium

3.1.1. Influence of μ_a/μ_s'. A cubic-shaped phantom is considered with a size of 10 mm $\times$ 10 mm $\times$ 10 mm, as shown in figure 1(a), which can be used to mimic the small animal brain. The 3D solid is discretized with a FE mesh of 4851 nodes and 20 000 tetrahedral elements. A point source with unit strength 1 is located at position $x = 0$ mm, $y = 5$ mm and $z = 5$ mm. Vacuum BC is enforced for the entire surfaces, in which the boundary coefficient α for type III BCs is specified as 0.467. It is well known that the first-order diffusion equation requires $(\mu_a/\mu_s') \ll 1$. To study when the first-order diffusion model cannot meet the accuracy requirements in the case of μ_a/μ_s' reaching to 1, or even greater than 1, a series of tests using first-order or higher order diffusion equations are performed for different values of this ratio. For all the test cases, the scattering coefficient is 1.0 mm^{-1} with $g = 0$ ($\mu_s' = \mu_s$). The absorption coefficient varies from 0.1 mm^{-1}, 1.0 mm^{-1} to 2 mm^{-1} for simulating blood vessel or other soft tissues, which results in the ratio of μ_a/μ_s' between 0.1 and 2. Figure 1(b) displays the calculated results of photon density for different absorption coefficients using the two models along the line ($y = 5$ mm, $z = 5$ mm). It is observed that first-order and higher order diffusion equations yield almost the same results when the ratio is equal to 0.1. However, with the increasing absorption, first-order diffusion theory progressively underestimates the photon density. Additionally, it is also shown in figure 1(b) that the difference between the first-order or higher order diffusion equations increases with increasing distance from the source. These observations agree well with the results from both s_n method and 2D p_n approximation (Hielscher *et al* 1998, Aydin *et al* 2002).

3.1.2. Influence of the anisotropy factor g. The influence of different g values on the photon transport in tissue is investigated for a homogeneous background region, as shown in figure 1(a). Figure 1(c) shows the ratio of the photon density calculated from a homogenous media with $\mu_s = 2.0$, $g = 0.5$ and $\mu_s = 1.0$, $g = 0$ based on various values of μ_a. It is noted that

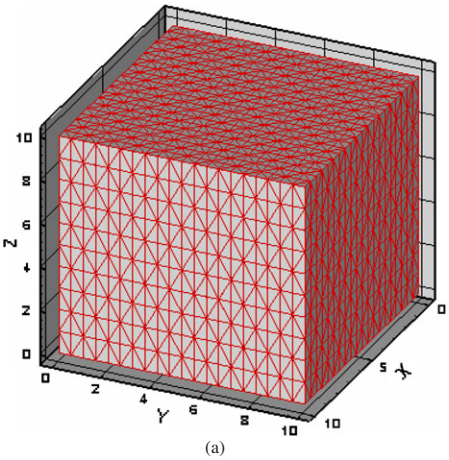

(a)

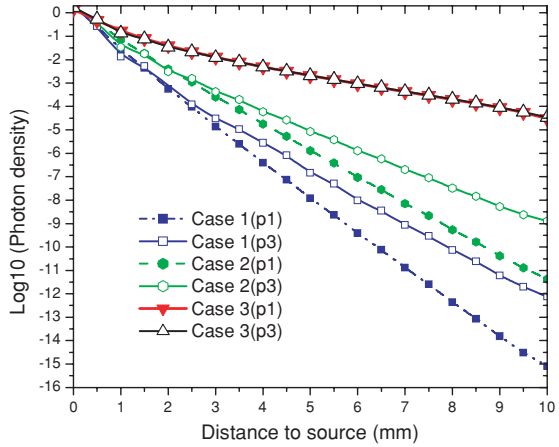

(b)

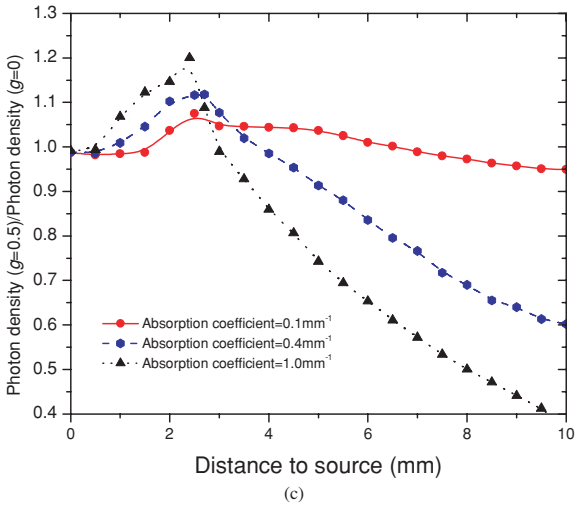

(c)

Figure 1. (a) Test geometry for a homogeneous medium. (b) Calculated photon density in the logarithmic scale using the first-order diffusion equation (p_1) and higher order diffusion equations (p_3) with, $\mu_a/\mu_s' = 2$ (case 1), $\mu_a/\mu_s' = 1$ (case 2) and $\mu_a/\mu_s' = 0.1$ (case 3). (c) Influence of factor g on the photon density for various absorption coefficients.

the first-order diffusion equation should give the same results for these two cases. However, the higher order diffuse equations provide quite different results for media with different factor g. It is observed in figure 1(c) that when the first-order approximation is valid (i.e., $\mu_a = 0.1$ mm^{-1} here), the difference between the two cases is not significant and the ratio almost approaches 1. Conversely, with increased optical absorption coefficients (i.e., $\mu_a = 0.4$ and 1 mm^{-1}), the first-order diffusion equation does not become valid and the consideration of g becomes important. We can see from figure 1(c) that for larger g values photon density distribution exhibits a clear maximum at the distance about 2 mm from the source and then a substantial decrease further from this peak point.

3.2. Heterogeneous medium

3.2.1. Influence of μ_a/μ_s'. We now investigated the differences between first-order diffusion theory and higher order diffusion theory for photon migration in a 3D heterogeneous medium. A box is considered as the background medium with a size of 20 mm × 20 mm × 1 mm and a cylindrical target ($(x-10)^2 + (y-10)^2 = 4$) is located at the center of the background medium, as shown in figure 2(a). The 3D solid is discretized with a FE mesh of 7803 nodes and 25 000 tetrahedral elements. A point source with unit strength 1 is located at position $x = 0.73$ mm, $y = 10$ mm and $z = 0.5$ mm. Type I BCs are imposed along all the surfaces for variables ψ_2, ψ_3, ψ_4, ψ_5 and ψ_6 while type III BCs are enforced for variable ψ_1 with $\alpha = 0.467$ along surfaces $y = 0$, $y = 20$ and $x = 20$. The scattering coefficient for the background medium and the target is specified as $\mu_s' = 2.0$ mm^{-1} with $g = 0$. The absorption coefficient for the background medium is $\mu_a = 0.01$ mm^{-1}. Three tests are performed when the optical absorption coefficient for the target are taken as $\mu_a = 0.1$ mm^{-1}, $\mu_a = 1.0$ mm^{-1} and $\mu_a = 3.0$ mm^{-1}, respectively. The calculated photon density are displayed in figure 2(b) along the line ($y = 10$ mm, $z = 0.5$ mm). It is observed from figure 2(b) that when $\mu_a = 0.1$ mm^{-1}, the first-order and higher order diffusion models agree well throughout the medium. However, for the other two cases, large differences between the two diffusion models can be observed inside the target zone while the two models match well in the background domain. The simulation results in figure 2(b) indicated that when μ_a/μ_s' approaches 1, even greater than 1 in the target zone, the first-order diffusion theory overestimates the photon density in the heterogeneous medium by more than two orders of magnitude. From the results we can say that the first-order diffusion model is not accurate enough to describe photon migration inside blood vessels of organs with a high blood perfusion, such as liver. The results also agree well with the results from both s_n method and 2D p_n approximation (Hielscher *et al* 1998, Aydin *et al* 2002). Recently another model was developed to describe 3D photon propagation based on sp_n approximation (Klose and Larson 2006). Though this model seems elegant, it may be difficult to solve the developed equations using the FE method, while it is certain that higher accuracy can be expected with an increased order of sp_n approximation.

3.2.2. Influence of the non-scattering, void-like region. Major concern is encountered in how light propagation is influenced by scattering- and absorption-free regions including void-like domain or a clear, non-scattering layer of cerebrospinal fluid. As a new investigation, a box background medium, as shown in figure 1(a), contains a spherical target with a diameter of 2 mm ($(x-5)^2 + (y-5)^2 + (z-5)^2 = 1$). The FEM mesh and BCs as well as source term are the same with the tests in section 3.1. The optical properties within the sphere target ($\mu_a = 0.000\,01$ mm^{-1}, $\mu_s' = 0.01$ mm^{-1}) are much lower than in the surrounding medium ($\mu_a = 0.005$ mm^{-1}, $\mu_s' = 0.5$ mm^{-1}). The optical properties of the two regions are chosen to ensure that the first-order diffusion approximation holds according to the criteria $\mu_a/\mu_s' \ll 1$,

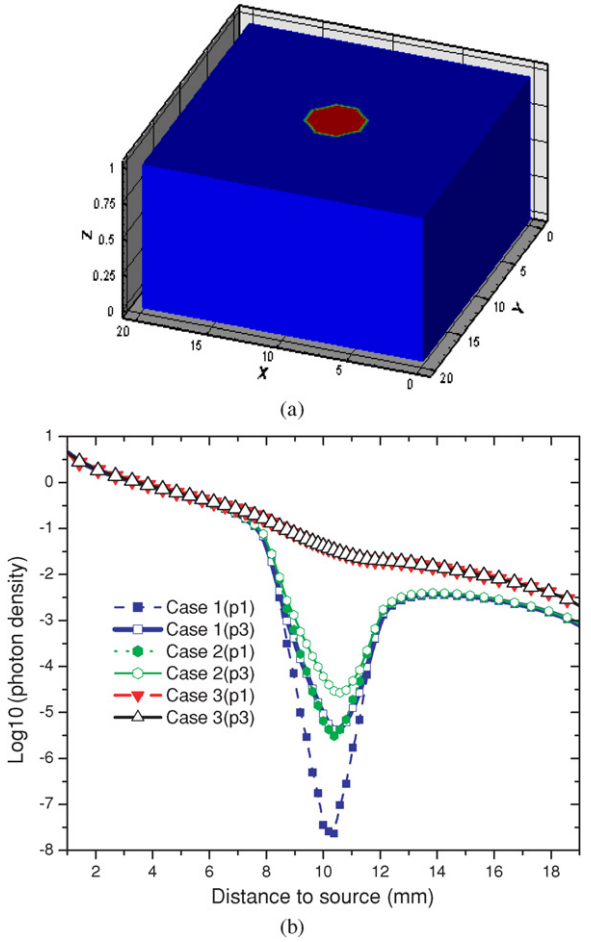

Figure 2. (a) Test geometry for a heterogeneous medium. (b) Calculated photon density in logarithmic scale using the first-order diffusion equation (p_1) and higher order diffusion equations (p_3) with $\mu_a/\mu_s' = 1.5$ (case 1), $\mu_a/\mu_s' = 0.5$ (case 2) and $\mu_a/\mu_s' = 0.05$ (case 3) inside the target region.

everywhere in the medium. The simulating results are plotted in figure 3 along the line ($y = 5$, $z = 5$ mm). It is observed from figure 3 that the differences between the first-order and higher order diffusion models do occur. In the void-like region with very low scattering and absorption, the first-order diffusion calculations predict an almost constant photon density. Just before this region, first-order diffusion theory predicts a photon density smaller than higher order theory, and just behind this region, the first-order diffusion theory predicts a photon density higher than higher order theory. This phenomenon agrees well with the results from both s_n method and 2D p_n approximation (Hielscher *et al* 1998, Aydin *et al* 2002). These results are expected because of geometry effects inside the void region. This observation also indicates that the boundaries between two media with quite different optical properties have a larger effect on the calculated results. For such cases, the first-order approximation cannot give satisfactory results even if $\mu_a/\mu_s' \ll 1$ is satisfied everywhere. Here the higher order model serves the job better likely because of its ability to model photon angular distributions.

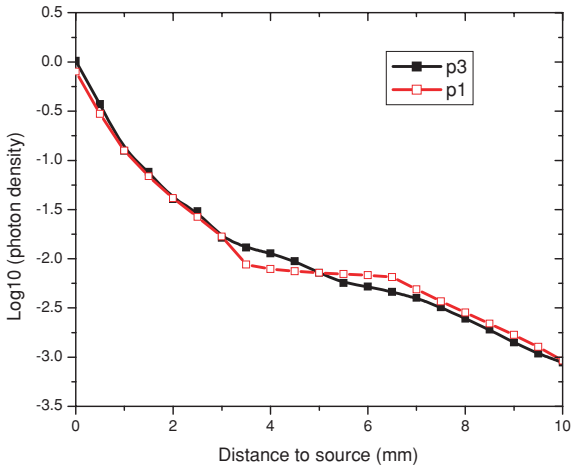

Figure 3. Comparison of Log_{10} of the photon density modeled with the first-order diffusion equation (p_1) and higher order diffusion equations (p_3) in a medium that contains a scattering- and absorption-free sphere.

3.3. Comparison with MC simulations

In this part, the comparison between the MC simulations and the FE numerical results from the higher and first-order diffusion models is presented. The geometry for the simulation tests is shown in figure 4(a). In our tests, a 20 mm diameter cylinder (height: 20 mm) was used as the background medium. One centered 10 mm diameter cylindrical object was embedded in the background medium. The optical properties for the background medium were $\mu_a = 0.01\ \mathrm{mm}^{-1}$ and $\mu_s' = 1.0\ \mathrm{mm}^{-1}$. The optical properties for the target were $\mu_a = 0.1\ \mathrm{mm}^{-1}$ and $\mu_s' = 1.0\ \mathrm{mm}^{-1}$ for test 1 and $\mu_a = 1.0\ \mathrm{mm}^{-1}$ and $\mu_s' = 1.0\ \mathrm{mm}^{-1}$ for test 2. For FE numerical computation, the simulations were performed with a uniform mesh of 6347 nodes and 27 840 tetrahedral elements. For MC simulations, the reflective index for the background and the target is assumed to be 1.0 and 1.4, respectively. The incident beam diameter is 0 with the photon incident point ($x = -10$, $y = 0$, $z = 10$ mm), and the anisotropy factor $g = 0.0$. The normalized results along the line $y = 0$ and $z = 10.0$ for FE and MC simulations are provided in figures 4(b) and (c). The MC method provides a statistical simulation of photon migration and enables us to obtain the solution of the RTE under a Fresnel-based BC equivalent to the type III BC (Song *et al* 1999). Therefore, the simulation results are accurate enough to estimate the results from the approximation models. The comparison in figures 4(b) and (c) showed that solutions from higher order model agree well with those from MC simulations, which gives a good description of photon migration in a large range of conditions of interest for tissue optics. However, the first-order diffusion model cannot describe the photon migration effectively when μ_a/μ_s' approaches 1.

3.4. Image reconstruction using simulated finger joint systems: simulation test

We conducted simulations with joint-like configuration, as shown in figure 5(a). In this test, a 30 mm (diameter) $\times$ 20 mm (height) cylinder was used as the background medium. Two centered 10 mm diameter cylindrical objects, embedded in the background medium, were used to mimic bones. The spacing between the two 'bones' was 3.0 mm, which was used to simulate cartilage. The optical properties for the background and 'bones' were, respectively,

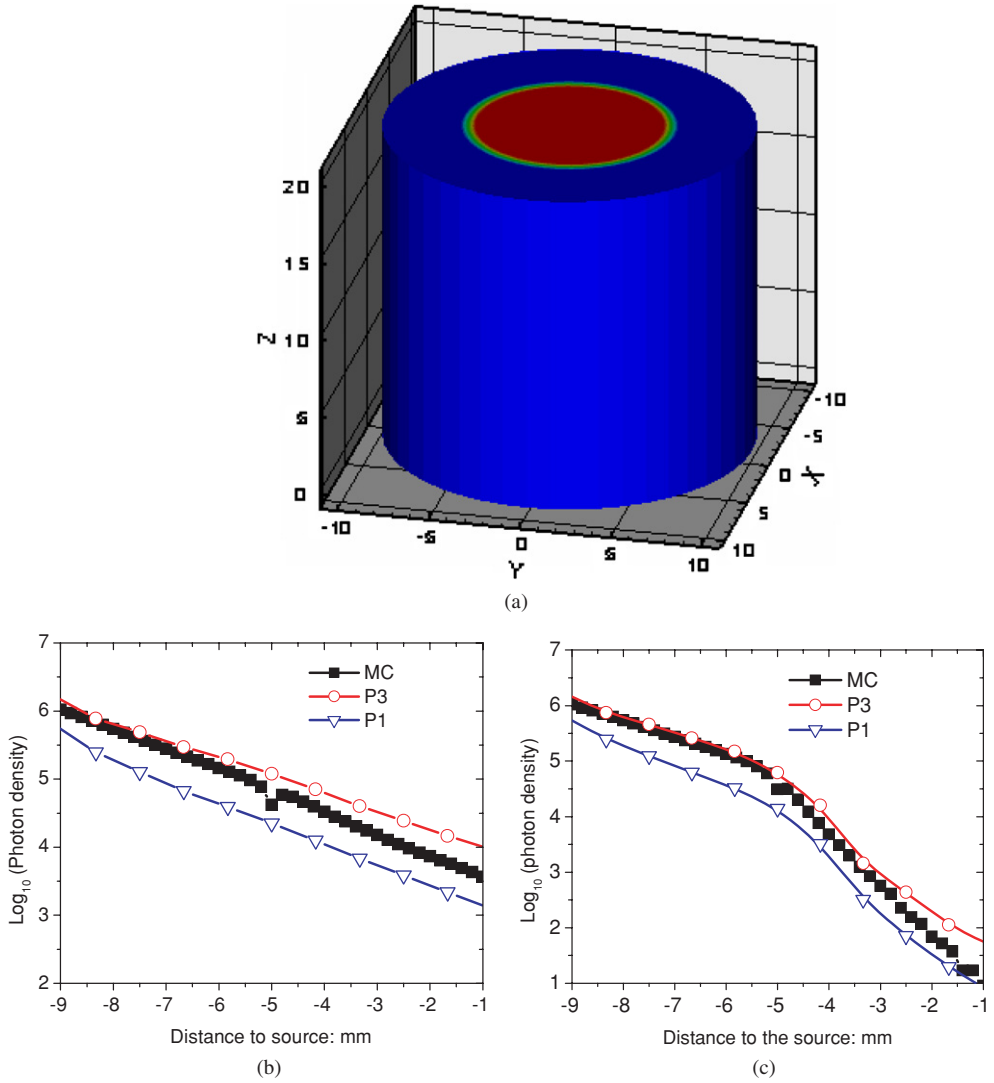

Figure 4. Simulation geometry used for MC, first-order and higher order diffusion modeling (a), comparison of Log_{10} of the photon density modeled using MC simulations, the first-order diffusion equation (p_1) and higher order diffusion equations (p_3) with $\mu_a/\mu_s' = 0.1$ (b) and $\mu_a/\mu_s' = 1$ (c).

$\mu_a = 0.01\ \mathrm{mm}^{-1}$ and $\mu_s' = 1.0\ \mathrm{mm}^{-1}$, and $\mu_a = 0.07\ \mathrm{mm}^{-1}$ and $\mu_s' = 2.0\ \mathrm{mm}^{-1}$, while the optical properties for the 'cartilage' were $\mu_a = 0.005\ \mathrm{mm}^{-1}$ and $\mu_s' = 0.5\ \mathrm{mm}^{-1}$. Additionally, 64 sources and 64 detectors were distributed uniformly along the surface of the background medium at four planes ($z = 2.5$, $z = 7.5$, $z = 12.5$ and $z = 17.5$ mm; 16 sources and 16 detectors at each plane). The 'measured' data were generated using the higher order diffusion models. To overcome the possible 'inverse crime' problem (Yuan *et al* 2007), we employed a fine mesh with 14 739 nodes and 79 680 tetrahedral elements to generate the 'measured' data and a coarse mesh with 2109 nodes and 8960 tetrahedral elements for the inverse computation.

In addition, we have developed a regularization-based FE reconstruction algorithm coupled with an optimization scheme that allows for determining optimized initial parameters

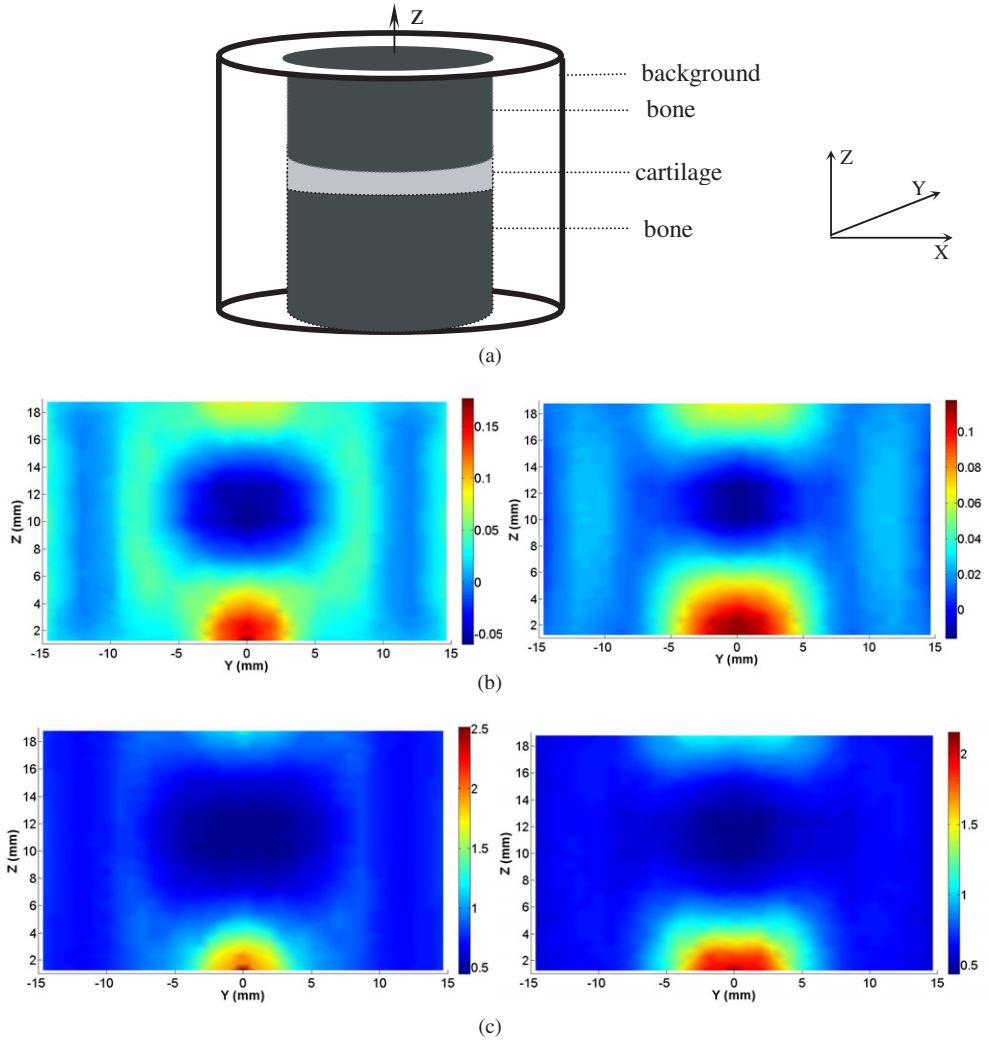

Figure 5. Test geometry mimicking a finger joint (a), reconstructed images at the $x = 0$ plane from simulated data using the first-order (left column) and higher order diffusion models (right column): (b) absorption images and (c) scattering images.

needed for reconstruction (Iftimia and Jiang 2000). Our reconstruction method has been previously tested and evaluated using extensive phantom and *in vivo* data (Jiang *et al* 2000, 2001). High-quality image reconstruction based on the above iterative procedure depends on good choice of four initial parameters including the BC coefficient α, the source strength S and the initial guesses of D and μ_α. The existing optimization scheme (Iftimia and Jiang 2000) we developed is based on the forward computation of the diffusion equation so that the following objective function is minimized:

$$\text{Min} : \mathbf{F} = \sum_{i=1}^{M} \left(\psi_i^m - \psi_i^c\right)^2 \tag{31}$$

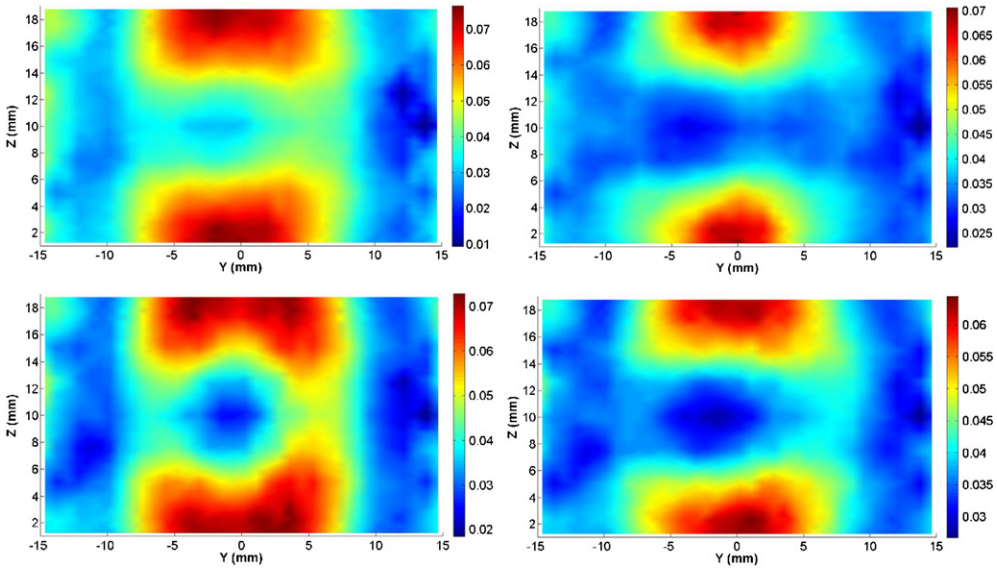

Figure 6. Reconstructed absorption images at the $x = 0$ and $x = 3$ planes from the experimental test using the first-order (left column) and higher order models (right column).

where ψ_i^m is the measured photon density from a given experimental inhomogeneous medium, and ψ_i^c is the computed photon density from a homogeneous medium with the same geometry based on the first-order or higher order diffuse model.

Figures 5(b) and (c) present the reconstructed absorption and scattering images at a selected longitudinal plane $x = 0$ mm using the first-order (left column) and the higher order diffusion model (right column).

3.5. Image reconstruction using simulated finger joint systems: phantom experiment

In our phantom experiment, a 30 mm diameter cylindrical solid phantom was used as the background medium. Two 15 mm diameter cylindrical solid objects (3 mm off z-axis) mimicking bones were embedded in the background medium, as schematically displayed in figure 5(a). The spacing ('cartilage') between the two 'bones' was 2.5 mm. The phantom materials used consisted of Intralipid as scatterer and India ink as absorber with Agar powder (1–2%) for solidifying the Intralipid and India ink solution. The experimental setup has been described elsewhere (Yuan *et al* 2007, 2008). The source and detector distributions are the same as the simulation tests mentioned above. The optical properties for the background were $\mu_a = 0.01$ mm^{-1} and $\mu_s' = 1.0$ mm^{-1} while the optical properties of the 'cartilage' were assumed to have the same values as the background medium. The optical properties for the 'bones' involved were $\mu_a = 0.07$ mm^{-1} and $\mu_s' = 4.0$ mm^{-1}. The recovered absorption images using the first-order (left column) and higher order (right column) diffusion equations are shown in figure 6 (since the scattering images from the first-order and higher order models do not show a significant difference, they are not provided here). For the reconstructions using phantom data, the first-order and higher order models-based algorithms require, respectively, 9.0 and 15.0 min per iteration when a FE mesh of 3009 nodes with 12 800 tetrahedral elements solver is used.

4. Discussion

We employed a 3D FE-p_3 approximated higher order diffusion model to investigate the photon migration in homogeneous and heterogeneous turbid media. We investigated the limits of the first-order diffusion model in small-volume tissues where diffusion approximation may become less attractive and BC effects are significant. We observed that when the first-order diffusion approximation condition $\mu_a/\mu_s' \ll 1$ is not satisfied, the first-order theory overestimates the absorption effects for a homogeneous medium. First-order diffusion calculations predict for such a case a much stronger decay of photon density than that from high-order calculations. In addition, we observed that first-order diffusion theory also overestimates the absorption effects of a heterogeneous medium when the absorption coefficients are approaching its scattering coefficient in target domain. We also found that the first-order diffusion model is not effective enough to describe photon migration in a region with low optical properties. Further, it should be pointed out that the solutions from the developed 3D p_3 approximated diffusion model agree well with those from MC simulations.

From figure 5, we can see that both absorption and scattering images are well recovered in terms of the separation of 'bones' and 'cartilage', position, shape and optical property values of each target by the first-order and higher order diffusion models. However, the optical images are considerably better reconstructed using the higher order model. It seems from the left columns of figures 5(b) and (c) that when low-absorption and low-scattering 'cartilage' (relative to the background) are present in the joint, the first-order model overestimates the size of the gap and underestimates the size of the bones. In addition, we note from figure 5 that the first-order model underestimates the absorption coefficient value of the joint and overestimates both the absorption and scattering coefficient values of the bones. Here we see that while both the first-order and higher order models based algorithms can provide effective image reconstructions for the finger joints, it appears that the higher order model described can quantitatively improve the reconstruction quality of both absorption and scattering images.

From figure 6, we see that the reconstruction quality of absorption images is enhanced when the higher order model-based algorithm (right column, figure 6) is used, while the optical images can be reconstructed with the first-order diffusion model (left column, figure 6). For example, the absorption images have smaller background artifacts and are more accurately recovered especially in the 'cartilage' region in terms of the shape and optical property value of the 'cartilage' when the higher order model was used. We also observe that when the optical properties of the 'cartilage' are equal to those of the background, the first-order diffuse model overestimates the optical absorption coefficient of the 'cartilage'.

In summary, in this paper we have derived 3D higher order diffusion equations. We have also validated this model using MC simulations. Reconstructions based on both the first-order and higher order diffusion equations using both simulated and tissue phantom data have been conducted and the results indicate that the higher order model can indeed effectively image small tissue volumes such as the finger joints and can quantitatively improve 3D DOT image reconstructions.

5. Summary

Transport equation is very accurate to model photon propagation in biological tissues. However, it is very difficult to solve the equation due to its complex mathematical forms and BCs. As such, a simplified spherical harmonics approximated higher order diffuse model is derived, which can be easily solved by the FE method with high numerical accuracy and low computation cost. According to forward tests, we conclude that the developed higher

order diffusion model is able to accurately describe light propagation in biological tissues and the solutions agree well with those from MC simulations. In addition, the developed model is also validated by inverse reconstruction computation in optical tomography. Using imaging in small-volume tissues as an example, we observed significant differences between the reconstructed results from the first-order and higher order diffusion equations.

Appendix

The moment equations derived from the p_3 approximated RTE are written as

$l = 0$, $m = 0$:

$$2\frac{\partial \psi_{10}}{\partial z} + 2\left(\frac{\partial \psi_{11}}{\partial x} + \frac{\partial \gamma_{11}}{\partial y}\right) + 2\sigma_{00}\psi_{00} = s \tag{A.1}$$

$$2\frac{\partial \gamma_{10}}{\partial z} + 2\left(-\frac{\partial \psi_{11}}{\partial y} + \frac{\partial \gamma_{11}}{\partial x}\right) = 0 \tag{A.2}$$

$l = 1$, $m = 1$:

$$6\frac{\partial \psi_{21}}{\partial z} + 2\frac{\partial \psi_{00}}{\partial x} - 2\frac{\partial \psi_{20}}{\partial x} + 12\left(\frac{\partial \psi_{22}}{\partial x} + \frac{\partial \gamma_{22}}{\partial y}\right) + 6\sigma_{11}\psi_{11} = 0 \tag{A.3}$$

$$6\frac{\partial \gamma_{21}}{\partial z} + 2\frac{\partial \psi_{00}}{\partial y} - 2\frac{\partial \psi_{20}}{\partial y} + 12\left(-\frac{\partial \psi_{22}}{\partial y} + \frac{\partial \gamma_{22}}{\partial x}\right) + 6\sigma_{11}\gamma_{11} = 0 \tag{A.4}$$

$l = 1$, $m = 0$:

$$2\frac{\partial \psi_{00}}{\partial z} + 4\frac{\partial \psi_{20}}{\partial z} + 6\left(\frac{\partial \psi_{21}}{\partial x} + \frac{\partial \gamma_{21}}{\partial y}\right) + 6\sigma_{10}\psi_{10} = 0 \tag{A.5}$$

$$6\left(-\frac{\partial \psi_{21}}{\partial y} + \frac{\partial \gamma_{21}}{\partial x}\right) = 0 \tag{A.6}$$

$l = 2$, $m = 1$:

$$2\frac{\partial \psi_{11}}{\partial z} + 8\frac{\partial \psi_{31}}{\partial z} + 2\frac{\partial \psi_{10}}{\partial x} - 2\frac{\partial \psi_{30}}{\partial x} + 20\left(\frac{\partial \psi_{32}}{\partial x} + \frac{\partial \gamma_{32}}{\partial y}\right) + 10\sigma_{21}\psi_{21} = 0 \tag{A.7}$$

$$2\frac{\partial \gamma_{11}}{\partial z} + 8\frac{\partial \gamma_{31}}{\partial z} + 2\frac{\partial \psi_{10}}{\partial y} - 2\frac{\partial \psi_{30}}{\partial y} + 20\left(-\frac{\partial \psi_{32}}{\partial y} + \frac{\partial \gamma_{32}}{\partial x}\right) + 10\sigma_{21}\gamma_{21} = 0 \tag{A.8}$$

$l = 2$, $m = 2$:

$$10\frac{\partial \psi_{32}}{\partial z} + \left(\frac{\partial \psi_{11}}{\partial x} - \frac{\partial \gamma_{11}}{\partial y}\right) - \left(\frac{\partial \psi_{31}}{\partial x} - \frac{\partial \gamma_{31}}{\partial y}\right) + 30\left(\frac{\partial \psi_{33}}{\partial x} + \frac{\partial \gamma_{33}}{\partial y}\right) + 10\sigma_{22}\psi_{22} = 0 \tag{A.9}$$

$$10\frac{\partial \gamma_{32}}{\partial z} + \left(\frac{\partial \psi_{11}}{\partial y} + \frac{\partial \gamma_{11}}{\partial x}\right) - \left(\frac{\partial \psi_{31}}{\partial y} + \frac{\partial \gamma_{31}}{\partial x}\right) + 30\left(-\frac{\partial \psi_{33}}{\partial y} + \frac{\partial \gamma_{33}}{\partial x}\right) + 10\sigma_{22}\gamma_{22} = 0 \tag{A.10}$$

l = 2, *m* = 0:

$$6\frac{\partial\psi_{30}}{\partial z}+4\frac{\partial\psi_{10}}{\partial z}+12(\frac{\partial\psi_{31}}{\partial x}+\frac{\partial\gamma_{31}}{\partial y})-2\left(\frac{\partial\psi_{11}}{\partial x}+\frac{\partial\gamma_{11}}{\partial y}\right)+10\sigma_{20}\psi_{20}=0 \tag{A.11}$$

$$6\frac{\partial\gamma_{30}}{\partial z}+4\frac{\partial\gamma_{10}}{\partial z}+12\left(-\frac{\partial\psi_{31}}{\partial y}+\frac{\partial\gamma_{31}}{\partial x}\right)-2\left(-\frac{\partial\psi_{11}}{\partial y}+\frac{\partial\gamma_{11}}{\partial x}\right)+10\sigma_{20}\gamma_{20}=0 \tag{A.12}$$

l = 3, *m* = 3:

$$\left(\frac{\partial\psi_{22}}{\partial x}-\frac{\partial\gamma_{22}}{\partial y}\right)+14\sigma_{33}\psi_{33}=0 \tag{A.13}$$

$$\left(\frac{\partial\psi_{22}}{\partial y}+\frac{\partial\gamma_{22}}{\partial x}\right)+14\sigma_{33}\gamma_{33}=0 \tag{A.14}$$

l = 3, *m* = 1:

$$4\frac{\partial\psi_{21}}{\partial z}+2\frac{\partial\psi_{20}}{\partial x}-2\left(\frac{\partial\psi_{22}}{\partial x}+\frac{\partial\gamma_{22}}{\partial y}\right)+14\sigma_{31}\psi_{31}=0 \tag{A.15}$$

$$4\frac{\partial\gamma_{21}}{\partial z}+2\frac{\partial\psi_{20}}{\partial y}-2\left(-\frac{\partial\psi_{22}}{\partial y}+\frac{\partial\gamma_{22}}{\partial x}\right)+14\sigma_{31}\gamma_{31}=0 \tag{A.16}$$

l = 3, *m* = 2:

$$2\frac{\partial\psi_{22}}{\partial z}+\left(\frac{\partial\psi_{21}}{\partial x}-\frac{\partial\gamma_{21}}{\partial y}\right)+14\sigma_{32}\psi_{32}=0 \tag{A.17}$$

$$2\frac{\partial\gamma_{22}}{\partial z}+\left(\frac{\partial\psi_{21}}{\partial y}+\frac{\partial\gamma_{21}}{\partial x}\right)+14\sigma_{32}\gamma_{32}=0 \tag{A.18}$$

l = 3, *m* = 0:

$$6\frac{\partial\psi_{20}}{\partial z}-6\left(\frac{\partial\psi_{21}}{\partial x}+\frac{\partial\gamma_{21}}{\partial y}\right)+14\sigma_{30}\psi_{30}=0. \tag{A.19}$$

Taking the partial derivative of equation (A.3) with respect to x and equation (A.4) with respect to y,

$$6\frac{\partial^2\psi_{21}}{\partial z\partial x}+2\frac{\partial^2\psi_{00}}{\partial^2 x}-2\frac{\partial^2\psi_{20}}{\partial^2 x}+12\left(\frac{\partial^2\psi_{22}}{\partial^2 x}+\frac{\partial^2\gamma_{22}}{\partial y\partial x}\right)+6\sigma_{11}\frac{\partial\psi_{11}}{\partial x}=0 \tag{A.20}$$

$$6\frac{\partial^2\gamma_{21}}{\partial z\partial y}+2\frac{\partial^2\psi_{00}}{\partial^2 y}-2\frac{\partial^2\psi_{20}}{\partial^2 y}+12\left(-\frac{\partial^2\psi_{22}}{\partial^2 y}+\frac{\partial^2\gamma_{22}}{\partial x\partial y}\right)+6\sigma_{11}\frac{\partial\gamma_{11}}{\partial y}=0. \tag{A.21}$$

Adding equations (A.20) and (A.21),

$$\begin{aligned}6\frac{\partial^2\psi_{21}}{\partial z\partial x}+2\frac{\partial^2\psi_{00}}{\partial^2 x}-2\frac{\partial^2\psi_{20}}{\partial^2 x}+12\left(\frac{\partial^2\psi_{22}}{\partial^2 x}+\frac{\partial^2\gamma_{22}}{\partial y\partial x}\right)+6\sigma_{11}\left(\frac{\partial\psi_{11}}{\partial x}+\frac{\partial\gamma_{11}}{\partial y}\right)\\+6\frac{\partial^2\gamma_{21}}{\partial z\partial y}+2\frac{\partial^2\psi_{00}}{\partial^2 y}-2\frac{\partial^2\psi_{20}}{\partial^2 y}+12\left(-\frac{\partial^2\psi_{22}}{\partial^2 y}+\frac{\partial^2\gamma_{22}}{\partial x\partial y}\right)=0\end{aligned} \tag{A.22}$$

and then combining equation (A.1)

$$2\left(\frac{\partial\psi_{11}}{\partial x}+\frac{\partial\gamma_{11}}{\partial y}\right)=s-2\sigma_{00}\psi_{00}-2\frac{\partial\psi_{10}}{\partial z} \tag{A.23}$$

with equation (A.5),

$$2\left(\frac{\partial^2\psi_{21}}{\partial x\partial z}+\frac{\partial^2\gamma_{21}}{\partial y\partial z}\right)+\frac{2}{3}\frac{\partial^2\psi_{00}}{\partial^2 z}+\frac{4}{3}\frac{\partial^2\psi_{20}}{\partial^2 z}+2\sigma_{10}\frac{\partial\psi_{10}}{\partial z}=0, \tag{A.24}$$

we obtain

$$2\left(\frac{\partial\psi_{11}}{\partial x}+\frac{\partial\gamma_{11}}{\partial y}\right)=s-2\sigma_{00}\psi_{00}+\frac{1}{\sigma_{10}}\left(\frac{2}{3}\frac{\partial^2\psi_{00}}{\partial^2 z}+\frac{4}{3}\frac{\partial^2\psi_{20}}{\partial^2 z}+2\left(\frac{\partial^2\psi_{21}}{\partial x\partial z}+\frac{\partial^2\gamma_{21}}{\partial y\partial z}\right)\right). \tag{A.25}$$

On substituting equation (A.25) into equation (A.22) and assuming $\sigma_{10}=\sigma_{11}$, we get

$$\frac{2}{3}\left(\frac{\partial^2\psi_{00}}{\partial^2 x}+\frac{\partial^2\psi_{00}}{\partial^2 y}+\frac{\partial^2\psi_{00}}{\partial^2 z}\right)+\left(\frac{4}{3}\frac{\partial^2\psi_{20}}{\partial^2 z}-\frac{2}{3}\frac{\partial^2\psi_{20}}{\partial^2 x}-\frac{2}{3}\frac{\partial^2\psi_{20}}{\partial^2 y}\right)+4\left(\frac{\partial^2\psi_{22}}{\partial^2 x}\right)+4\frac{\partial^2\psi_{21}}{\partial z\partial x}$$
$$+4\frac{\partial^2\gamma_{21}}{\partial z\partial y}+4\left(-\frac{\partial^2\psi_{22}}{\partial^2 y}\right)+8\frac{\partial^2\gamma_{22}}{\partial x\partial y}+\sigma_{11}(s-2\sigma_{00}\psi_{00})=0. \tag{A.26}$$

Equation (A.26) is our first governing equation for the 3D p_3 approximation to RTE. Now we try to derive the other five governing equations below. We take the partial derivative of equation (A.15) by x and equation (A.16) by y,

$$4\frac{\partial^2\psi_{21}}{\partial z\partial x}+2\frac{\partial^2\psi_{20}}{\partial^2 x}-2\left(\frac{\partial^2\psi_{22}}{\partial^2 x}+\frac{\partial^2\gamma_{22}}{\partial y\partial x}\right)+14\sigma_{31}\frac{\partial\psi_{31}}{\partial x}=0 \tag{A.27}$$

$$4\frac{\partial^2\gamma_{21}}{\partial z\partial y}+2\frac{\partial^2\psi_{20}}{\partial^2 y}-2\left(-\frac{\partial^2\psi_{22}}{\partial^2 y}+\frac{\partial^2\gamma_{22}}{\partial x\partial y}\right)+14\sigma_{31}\frac{\partial\gamma_{31}}{\partial y}=0. \tag{A.28}$$

Adding equations (A.27) and (A.28), we get

$$4\frac{\partial^2\psi_{21}}{\partial z\partial x}+2\frac{\partial^2\psi_{20}}{\partial^2 x}-2\left(\frac{\partial^2\psi_{22}}{\partial^2 x}+\frac{\partial^2\gamma_{22}}{\partial y\partial x}\right)+14\sigma_{31}\left(\frac{\partial\psi_{31}}{\partial x}+\frac{\partial\gamma_{31}}{\partial y}\right)+4\frac{\partial^2\gamma_{21}}{\partial z\partial y}+2\frac{\partial^2\psi_{20}}{\partial^2 y}$$
$$-2\left(-\frac{\partial^2\psi_{22}}{\partial^2 y}+\frac{\partial^2\gamma_{22}}{\partial x\partial y}\right)=0. \tag{A.29}$$

Note that equation (A.11) can be written as

$$12\left(\frac{\partial\psi_{31}}{\partial x}+\frac{\partial\gamma_{31}}{\partial y}\right)=2\left(\frac{\partial\psi_{11}}{\partial x}+\frac{\partial\gamma_{11}}{\partial y}\right)-10\sigma_{20}\psi_{20}-4\frac{\partial\psi_{10}}{\partial z}-6\frac{\partial\psi_{30}}{\partial z}. \tag{A.30}$$

Also note that equation (A.22) can be further written as

$$-\frac{1}{6\sigma_{11}}\left\{6\frac{\partial^2\psi_{21}}{\partial z\partial x}+2\frac{\partial^2\psi_{00}}{\partial^2 x}-2\frac{\partial^2\psi_{20}}{\partial^2 x}+12\left(\frac{\partial^2\psi_{22}}{\partial^2 x}+\frac{\partial^2\gamma_{22}}{\partial y\partial x}\right)+6\frac{\partial^2\gamma_{21}}{\partial z\partial y}+2\frac{\partial^2\psi_{00}}{\partial^2 y}-2\frac{\partial^2\psi_{20}}{\partial^2 y}\right.$$
$$\left.+12\left(-\frac{\partial^2\psi_{22}}{\partial^2 y}+\frac{\partial^2\gamma_{22}}{\partial x\partial y}\right)\right\}=\left(\frac{\partial\psi_{11}}{\partial x}+\frac{\partial\gamma_{11}}{\partial y}\right). \tag{A.31}$$

We obtain the following equation after substituting equation (A.31) into equation (A.30):

$$\left(\frac{\partial\psi_{31}}{\partial x}+\frac{\partial\gamma_{31}}{\partial y}\right)=-\frac{5}{6}\sigma_{20}\psi_{20}-\frac{1}{36\sigma_{11}}\left[6\frac{\partial^2\psi_{21}}{\partial z\partial x}+2\frac{\partial^2\psi_{00}}{\partial^2 x}-2\frac{\partial^2\psi_{20}}{\partial^2 x}+12\left(\frac{\partial^2\psi_{22}}{\partial^2 x}+\frac{\partial^2\gamma_{22}}{\partial y\partial x}\right)\right.$$
$$\left.+6\frac{\partial^2\gamma_{21}}{\partial z\partial y}+2\frac{\partial^2\psi_{00}}{\partial^2 y}-2\frac{\partial^2\psi_{20}}{\partial^2 y}+12\left(-\frac{\partial^2\psi_{22}}{\partial^2 y}+\frac{\partial^2\gamma_{22}}{\partial x\partial y}\right)\right]-\frac{1}{3}\frac{\partial\psi_{10}}{\partial z}-\frac{1}{2}\frac{\partial\psi_{30}}{\partial z}. \tag{A.32}$$

Further, equation (A.5) can be rewritten as

$$\frac{1}{6\sigma_{10}}\left[2\left(\frac{\partial^2\psi_{21}}{\partial x\partial z}+\frac{\partial^2\gamma_{21}}{\partial y\partial z}\right)+\frac{2}{3}\frac{\partial^2\psi_{00}}{\partial^2 z}+\frac{4}{3}\frac{\partial^2\psi_{20}}{\partial^2 z}\right]=-\frac{1}{3}\frac{\partial\psi_{10}}{\partial z}. \tag{A.33}$$

Equation (A.19) can be rewritten as

$$\frac{1}{28\sigma_{30}}\left[6\frac{\partial^2\psi_{20}}{\partial^2 z}-6\left(\frac{\partial^2\psi_{21}}{\partial x\partial z}+\frac{\partial^2\gamma_{21}}{\partial y\partial z}\right)\right]=-\frac{1}{2}\frac{\partial\psi_{30}}{\partial z}. \tag{A.34}$$

Substituting equations (A.33) and (A.34) into equation (A.32),

$$\begin{aligned}\left(\frac{\partial\psi_{31}}{\partial x}+\frac{\partial\gamma_{31}}{\partial y}\right)=&\left\{-\frac{5}{6}\sigma_{20}\psi_{20}-\frac{1}{36\sigma_{11}}\left[6\frac{\partial^2\psi_{21}}{\partial z\partial x}+2\frac{\partial^2\psi_{00}}{\partial^2 x}-2\frac{\partial^2\psi_{20}}{\partial^2 x}+12\left(\frac{\partial^2\psi_{22}}{\partial^2 x}+\frac{\partial^2\gamma_{22}}{\partial y\partial x}\right)\right.\right.\\&\left.+6\frac{\partial^2\gamma_{21}}{\partial z\partial y}+2\frac{\partial^2\psi_{00}}{\partial^2 y}-2\frac{\partial^2\psi_{20}}{\partial^2 y}+12\left(-\frac{\partial^2\psi_{22}}{\partial^2 y}+\frac{\partial^2\gamma_{22}}{\partial x\partial y}\right)\right]\\&+\frac{1}{6\sigma_{10}}\left[2\left(\frac{\partial^2\psi_{21}}{\partial x\partial z}+\frac{\partial^2\gamma_{21}}{\partial y\partial z}\right)+\frac{2}{3}\frac{\partial^2\psi_{00}}{\partial^2 z}+\frac{4}{3}\frac{\partial^2\psi_{20}}{\partial^2 z}\right]\\&\left.+\frac{1}{28\sigma_{30}}\left[6\frac{\partial^2\psi_{20}}{\partial^2 z}-6\left(\frac{\partial^2\psi_{21}}{\partial x\partial z}+\frac{\partial^2\gamma_{21}}{\partial y\partial z}\right)\right]\right\}\end{aligned} \tag{A.35}$$

and equation (A.35) into equation (A.29), we obtain

$$\begin{aligned}&4\frac{\partial^2\psi_{21}}{\partial z\partial x}+2\frac{\partial^2\psi_{20}}{\partial^2 x}-2\left(\frac{\partial^2\psi_{22}}{\partial^2 x}+\frac{\partial^2\gamma_{22}}{\partial y\partial x}\right)+14\sigma_{31}\left\{-\frac{5}{6}\sigma_{20}\psi_{20}-\frac{1}{36\sigma_{11}}\left[6\frac{\partial^2\psi_{21}}{\partial z\partial x}+2\frac{\partial^2\psi_{00}}{\partial^2 x}\right.\right.\\&\quad-2\frac{\partial^2\psi_{20}}{\partial^2 x}+12\left(\frac{\partial^2\psi_{22}}{\partial^2 x}+\frac{\partial^2\gamma_{22}}{\partial y\partial x}\right)+6\frac{\partial^2\gamma_{21}}{\partial z\partial y}+2\frac{\partial^2\psi_{00}}{\partial^2 y}-2\frac{\partial^2\psi_{20}}{\partial^2 y}\\&\quad\left.+12\left(-\frac{\partial^2\psi_{22}}{\partial^2 y}+\frac{\partial^2\gamma_{22}}{\partial x\partial y}\right)\right]+\frac{1}{6\sigma_{10}}\left[2\left(\frac{\partial^2\psi_{21}}{\partial x\partial z}+\frac{\partial^2\gamma_{21}}{\partial y\partial z}\right)+\frac{2}{3}\frac{\partial^2\psi_{00}}{\partial^2 z}+\frac{4}{3}\frac{\partial^2\psi_{20}}{\partial^2 z}\right]\\&\quad\left.+\frac{1}{28\sigma_{30}}\left[6\frac{\partial^2\psi_{20}}{\partial^2 z}-6\left(\frac{\partial^2\psi_{21}}{\partial x\partial z}+\frac{\partial^2\gamma_{21}}{\partial y\partial z}\right)\right]\right\}\\&\quad+4\frac{\partial^2\gamma_{21}}{\partial z\partial y}+2\frac{\partial^2\psi_{20}}{\partial^2 y}-2\left(-\frac{\partial^2\psi_{22}}{\partial^2 y}+\frac{\partial^2\gamma_{22}}{\partial x\partial y}\right)=0.\end{aligned} \tag{A.36}$$

Equation (A.36) can be further written as

$$\begin{aligned}&\frac{50}{21}\left(\frac{\partial^2\psi_{20}}{\partial^2 x}+\frac{\partial^2\psi_{20}}{\partial^2 y}\right)+\frac{4}{3}\left(\frac{\partial^2\psi_{00}}{\partial^2 z}-\frac{1}{2}\frac{\partial\psi_{00}^2}{\partial^2 x}-\frac{1}{2}\frac{\partial\psi_{00}^2}{\partial^2 y}\right)+\frac{50}{21}\left(\frac{\partial^2\psi_{20}}{\partial^2 x}+\frac{\partial\psi_{20}^2}{\partial^2 y}\right)\\&\quad+\frac{40}{7}\left(\frac{\partial^2\psi_{22}}{\partial^2 y}-\frac{\partial^2\psi_{22}}{\partial x}-2\frac{\partial^2\gamma_{22}}{\partial x\partial y}\right)-10\sigma_{31}\sigma_{20}\psi_{20}+\frac{110}{21}\frac{\partial^2\psi_{20}}{\partial^2 z}\\&\quad+\frac{20}{7}\left(\frac{\partial^2\psi_{21}}{\partial z\partial x}+\frac{\partial^2\gamma_{21}}{\partial z\partial Y}\right)-10\sigma_{20}^2\psi_{22}=0.\end{aligned} \tag{A.37}$$

Equation (A.37) is the second governing equation for the 3D p_3 approximation.

Now we try to derive the third governing equation. From equation (A.9), we get

$$10\frac{\partial\psi_{32}}{\partial z}+\left(\frac{\partial\psi_{11}}{\partial x}-\frac{\partial\gamma_{11}}{\partial y}\right)-\left(\frac{\partial\psi_{31}}{\partial x}-\frac{\partial\gamma_{31}}{\partial y}\right)+30\left(\frac{\partial\psi_{33}}{\partial x}+\frac{\partial\gamma_{33}}{\partial y}\right)+10\sigma_{22}\psi_{22}=0. \tag{A.38}$$

Based on equations (A.20) and (A.21), we get

$$\left(\frac{\partial\psi_{11}}{\partial x}-\frac{\partial\gamma_{11}}{\partial y}\right)=\frac{1}{6\sigma_{11}}\left\{-\left[6\frac{\partial^2\psi_{21}}{\partial z\partial x}+2\frac{\partial^2\psi_{00}}{\partial^2 x}-2\frac{\partial^2\psi_{20}}{\partial^2 x}+12\left(\frac{\partial^2\psi_{22}}{\partial^2 x}+\frac{\partial^2\gamma_{22}}{\partial y\partial x}\right)\right]\right.$$
$$\left.+\left[6\frac{\partial^2\gamma_{21}}{\partial z\partial y}+2\frac{\partial^2\psi_{00}}{\partial^2 y}-2\frac{\partial^2\psi_{20}}{\partial^2 y}+12\left(-\frac{\partial^2\psi_{22}}{\partial^2 y}+\frac{\partial^2\gamma_{22}}{\partial x\partial y}\right)\right]\right\}. \tag{A.39}$$

From equations (A.15) and (A.16), we get

$$\frac{1}{14\sigma_{31}}\left\{\left[4\frac{\partial^2\psi_{21}}{\partial z\partial x}+2\frac{\partial^2\psi_{20}}{\partial^2 x}-2\left(\frac{\partial^2\psi_{22}}{\partial^2 x}+\frac{\partial^2\gamma_{22}}{\partial y\partial x}\right)\right]-\left[4\frac{\partial^2\gamma_{21}}{\partial z\partial y}+2\frac{\partial^2\psi_{20}}{\partial^2 y}\right.\right.$$
$$\left.\left.-2\left(-\frac{\partial^2\psi_{22}}{\partial^2 y}+\frac{\partial^2\gamma_{22}}{\partial x\partial y}\right)\right]\right\}=-\left(\frac{\partial\psi_{31}}{\partial x}-\frac{\partial\gamma_{31}}{\partial y}\right). \tag{A.40}$$

Taking the partial derivative of equation (A.13) with respect to x and equation (A.14) with respect to y, and then adding them gives

$$\left(\frac{\partial\psi_{33}}{\partial x}+\frac{\partial\gamma_{33}}{\partial y}\right)=\frac{1}{14\sigma_{33}}\left[-\left(\frac{\partial^2\psi_{22}}{\partial^2 y}+\frac{\partial^2\gamma_{22}}{\partial x\partial y}\right)-\left(\frac{\partial^2\psi_{22}}{\partial^2 x}-\frac{\partial^2\gamma_{22}}{\partial y\partial x}\right)\right]. \tag{A.41}$$

Substituting equations (A.9), (A.39)–(A.41) and taking the partial derivative of (A.17) with respect to z in equation (A.38), we obtain

$$\frac{1}{3}\left(\frac{\partial^2\psi_{00}}{\partial^2 x}-\frac{\partial^2\psi_{00}}{\partial^2 y}\right)-\frac{10}{21}\left(\frac{\partial^2\psi_{20}}{\partial^2 x}-\frac{\partial^2\psi_{20}}{\partial^2 y}\right)+\frac{10}{7}\left(\frac{\partial^2\psi_{21}}{\partial x\partial z}-\frac{\partial^2\gamma_{21}}{\partial y\partial z}\right)$$
$$+\frac{30}{7}\left(\frac{\partial\psi_{22}^2}{\partial^2 x}+\frac{\partial\psi_{22}^2}{\partial^2 y}+\frac{1}{3}\frac{\partial^2\psi_{22}}{\partial^2 z}\right)-10\sigma_{00}^2\psi_{22}=0. \tag{A.42}$$

This is the third governing equation for the 3D p_3 approximation of RTE. Additionally, based on equations (A.3) and (A.4), we obtain

$$6\frac{\partial^2\psi_{21}}{\partial z\partial y}+2\frac{\partial^2\psi_{00}}{\partial x\partial y}-2\frac{\partial^2\psi_{20}}{\partial x\partial y}+12\left(\frac{\partial\psi_{22}^2}{\partial x\partial y}+\frac{\partial^2\gamma_{22}}{\partial^2 y}\right)+6\sigma_{11}\left(\frac{\partial\psi_{11}}{\partial y}+\frac{\partial\gamma_{11}}{\partial x}\right)+6\frac{\partial^2\gamma_{21}}{\partial z\partial x}$$
$$+2\frac{\partial^2\psi_{00}}{\partial y\partial x}-2\frac{\partial^2\psi_{20}}{\partial y\partial x}+12\left(-\frac{\partial^2\psi_{22}}{\partial y\partial x}+\frac{\partial^2\gamma_{22}}{\partial^2 x}\right)=0. \tag{A.43}$$

From equations (A.15) and (A.16), we get

$$14\sigma_{31}\left(\frac{\partial\psi_{31}}{\partial y}+\frac{\partial\gamma_{31}}{\partial x}\right)=-\left[4\frac{\partial^2\gamma_{21}}{\partial z\partial x}+2\frac{\partial^2\psi_{20}}{\partial x\partial y}-2\left(-\frac{\partial^2\psi_{22}}{\partial y\partial x}+\frac{\partial^2\gamma_{22}}{\partial^2 x}\right)\right]$$
$$-\left[4\frac{\partial^2\psi_{21}}{\partial z\partial y}+2\frac{\partial^2\psi_{20}}{\partial x\partial y}-2\left(\frac{\partial^2\psi_{22}}{\partial x\partial y}+\frac{\partial^2\gamma_{22}}{\partial^2 y}\right)\right]. \tag{A.44}$$

From equations (A.13) and (A.14), we get

$$\left(\frac{\partial^2\psi_{22}}{\partial y\partial x}+\frac{\partial^2\gamma_{22}}{\partial^2 x}\right)+14\sigma_{33}\left(\frac{\partial\gamma_{33}}{\partial x}-\frac{\partial\psi_{33}}{\partial y}\right)-\left[\left(\frac{\partial^2\psi_{22}}{\partial x\partial y}-\frac{\partial^2\gamma_{22}}{\partial^2 y}\right)\right]=0. \tag{A.45}$$

Note that equations (A.43)–(A.45) can be further written as

$$\left(\frac{\partial\psi_{11}}{\partial y}+\frac{\partial\gamma_{11}}{\partial x}\right)=-\frac{1}{6\sigma_{11}}\left\{\left[6\frac{\partial^2\gamma_{21}}{\partial z\partial x}+2\frac{\partial^2\psi_{00}}{\partial y\partial x}-2\frac{\partial^2\psi_{20}}{\partial y\partial x}+12\left(-\frac{\partial^2\psi_{22}}{\partial y\partial x}+\frac{\partial^2\gamma_{22}}{\partial^2 x}\right)\right]\right.$$
$$\left.+\left[6\frac{\partial^2\psi_{21}}{\partial z\partial y}+2\frac{\partial^2\psi_{00}}{\partial x\partial y}-2\frac{\partial^2\psi_{20}}{\partial x\partial y}+12\left(\frac{\partial\psi_{22}^2}{\partial x\partial y}+\frac{\partial^2\gamma_{22}}{\partial^2 y}\right)\right]\right\} \tag{A.46}$$

$$-\left(\frac{\partial\psi_{31}}{\partial y}+\frac{\partial\gamma_{31}}{\partial x}\right)=\frac{1}{14\sigma_{31}}\left\{\left[4\frac{\partial^2\gamma_{21}}{\partial z\partial x}+\frac{\partial^2\psi_{20}}{\partial y\partial x}-2\left(-\frac{\partial^2\psi_{22}}{\partial y\partial x}+\frac{\partial^2\gamma_{22}}{\partial^2 x}\right)\right]+\left[4\frac{\partial^2\psi_{21}}{\partial z\partial y}+\frac{\partial^2\psi_{20}}{\partial x\partial y}-2\left(\frac{\partial^2\psi_{22}}{\partial x\partial y}+\frac{\partial^2\gamma_{22}}{\partial^2 y}\right)\right]\right\} \tag{A.47}$$

$$30\left(\frac{\partial\gamma_{33}}{\partial x}-\frac{\partial\psi_{33}}{\partial y}\right)=\frac{15}{7\sigma_{33}}\left\{\left[\left(\frac{\partial^2\psi_{22}}{\partial x\partial y}-\frac{\partial^2\gamma_{22}}{\partial^2 y}\right)\right]-\left[\left(\frac{\partial^2\psi_{22}}{\partial y\partial x}+\frac{\partial^2\gamma_{22}}{\partial^2 x}\right)\right]\right\}. \tag{A.48}$$

When equations (A.46)–(A.48) and the partial derivative of (A.17) with respect to z are substituted into equation (A.10), we obtain our fourth governing equation for the 3D p_3 approximation:

$$\frac{2}{3}\frac{\partial^2\psi_{00}}{\partial x\partial y}-\frac{20}{21}\frac{\partial^2\psi_{20}}{\partial x\partial y}+\frac{30}{7}\left(\frac{\partial\gamma_{22}^2}{\partial^2 x}+\frac{\partial\gamma_{22}^2}{\partial^2 y}+\frac{1}{3}\frac{\partial^2\gamma_{22}}{\partial^2 z}\right)+\frac{10}{7}\left(\frac{\partial^2\psi_{21}}{\partial y\partial z}+\frac{\partial\gamma_{21}^2}{\partial x\partial z}\right)-10\sigma_{00}^2\gamma_{22}=0. \tag{A.49}$$

Moreover, from equations (A.7) and (A.3), we obtain

$$\begin{aligned}&2\frac{\partial\psi_{11}}{\partial z}+8\frac{\partial\psi_{31}}{\partial z}+2\frac{\partial\psi_{10}}{\partial x}-2\frac{\partial\psi_{30}}{\partial x}+20\left(\frac{\partial\psi_{32}}{\partial x}+\frac{\partial\gamma_{32}}{\partial y}\right)+10\sigma_{21}\psi_{21}=0\\&2\frac{\partial\psi_{11}}{\partial z}=-\frac{1}{3\sigma_{11}}\left[6\frac{\partial\psi_{21}^2}{\partial^2 z}+2\frac{\partial^2\psi_{00}}{\partial x\partial z}-2\frac{\partial^2\psi_{20}}{\partial x\partial z}+12\left(\frac{\partial^2\psi_{22}}{\partial x\partial z}+\frac{\partial^2\gamma_{22}}{\partial y\partial z}\right)\right].\end{aligned} \tag{A.50}$$

Based on equation (A.15), we get

$$8\frac{\partial\psi_{31}}{\partial z}=-\frac{4}{7\sigma_{31}}\left[4\frac{\partial^2\psi_{21}}{\partial^2 z}+2\frac{\partial^2\psi_{20}}{\partial x\partial z}-2\left(\frac{\partial^2\psi_{22}}{\partial x\partial z}+\frac{\partial^2\gamma_{22}}{\partial y\partial z}\right)\right]. \tag{A.51}$$

From equation (A.19), we get

$$-2\frac{\partial\psi_{30}}{\partial x}=\frac{1}{7\sigma_{30}}\left[6\frac{\partial\psi_{20}^2}{\partial z\partial x}-6\left(\frac{\partial^2\psi_{21}}{\partial^2 x}+\frac{\partial^2\gamma_{21}}{\partial y\partial x}\right)\right]. \tag{A.52}$$

Based on equations (A.17) and (A.18), we get

$$20\left(\frac{\partial\psi_{32}}{\partial x}+\frac{\partial\gamma_{32}}{\partial y}\right)=-\frac{10}{7\sigma_{32}}\left\{\left[2\frac{\partial^2\psi_{22}}{\partial z\partial x}+\left(\frac{\partial^2\psi_{21}}{\partial^2 x}-\frac{\partial^2\gamma_{21}}{\partial y\partial x}\right)\right]+\left[2\frac{\partial^2\gamma_{22}}{\partial z\partial y}+\left(\frac{\partial^2\psi_{21}}{\partial^2 y}+\frac{\partial^2\gamma_{21}}{\partial x\partial y}\right)\right]\right\}. \tag{A.53}$$

From equation (A.5), we get

$$2\frac{\partial\psi_{10}}{\partial x}=-\frac{1}{3\sigma_{10}}\left[2\frac{\partial^2\psi_{00}}{\partial z\partial x}+4\frac{\partial^2\psi_{20}}{\partial z\partial x}+6\left(\frac{\partial^2\psi_{21}}{\partial^2 x}+\frac{\partial^2\gamma_{21}}{\partial y\partial x}\right)\right]. \tag{A.54}$$

As such, equation (A.7) is rewritten in consideration of equations (A.50)–(A.54):

$$\frac{4}{3}\frac{\partial^2\psi_{00}}{\partial x\partial z}+\frac{20}{21}\frac{\partial^2\psi_{20}}{\partial x\partial z}+\frac{30}{7}\left(\frac{\partial^2\psi_{21}}{\partial^2 z}+\frac{\partial^2\psi_{21}}{\partial^2 x}+\frac{1}{3}\frac{\psi_{21}^2}{\partial^2 y}\right)+\frac{40}{7}\left(\frac{\partial^2\psi_{22}}{\partial x\partial z}+\frac{\partial\gamma_{22}^2}{\partial y\partial z}+\frac{1}{2}\frac{\partial^2\gamma_{21}}{\partial z\partial y}\right)-10\sigma_{00}^2\psi_{21}=0. \tag{A.55}$$

This is the fifth governing equation for the 3D p_3 approximation. When similar derivations are performed for equation (A.8), we get our final governing equation for the 3D p_3 approximated RTE,

$$\frac{4}{3}\frac{\partial^2\psi_{00}}{\partial y\partial z}+\frac{20}{21}\frac{\partial^2\psi_{20}}{\partial y\partial z}+\frac{30}{7}\left(\frac{\partial^2\gamma_{21}}{\partial^2 z}+\frac{1}{3}\frac{\partial^2\gamma_{21}}{\partial^2 x}+\frac{\gamma_{21}^2}{\partial^2 y}\right)$$
$$+\frac{40}{7}\left(\frac{\partial^2\gamma_{22}}{\partial x\partial z}-\frac{\partial\psi_{22}^2}{\partial y\partial z}+\frac{1}{2}\frac{\partial^2\psi_{21}}{\partial x\partial y}\right)-10\sigma_{00}^2\gamma_{21}=0. \tag{A.56}$$

References

Aronson R and Corngold N 1999 Photon diffusion coefficient in the absorbing medium *J. Opt. Soc. Am.* A **16** 1066–71

Aydin E, Olivera C R E de and Goddard A J H 2004 A finite element-spherical harmonics radiation transport model for photon migration in turbid media *J. Quant. Radiat. Spectrosc. Transfer* **84** 247–60

Aydin E D, Oliveira C R E de and Goddard A J H 2002 A comparison between transport and diffusion calculations using a finite element-spherical harmonics radiation transport method *Med. Phys.* **29** 2013–23

Barbour R L, Graber H L, Wang Y, Chang J H and Aronson R 1993 A perturbation approach for optical diffusion tomography using continuous-wave and time-resolved data *Proc. SPIE* **IS11** 87–120

Boas D A 1995 Photon migration within the P3 approximation *Proc. SPIE* **2389** 240–47

Boverman G, Fang Q, Carp S, Miller E, Brook D, Selb J, Moore R, Kopans D and Boas D A 2007 Spatio-temporal imaging of the hemoglobin in the compressed breast with diffuse optical tomography *Phys. Med. Biol.* **52** 3619–41

Dehghani H, Delpy D and Arridge S 1999 Photon migration in non-scattering tissue and the effects on image reconstruction *Phys. Med. Biol.* **44** 2897–2906

Dorn A 1998 Transport—backtransport method for optical tomography *Inverse Problems* **14** 1107–30

Elaloufi R, Carminati R and Greffet J 2003 Definition of diffusion coefficient in scattering and absorbing media *J. Opt. Soc. Am* A **20** 678–85

Golub Gene H and Loan Charles F Van 1996 *Matrix Computation* (Baltimore, MD: John Hopkins University Press)

Hebden J, Arridge S and Delpy D 1997 Optical imaging in medicine: I. Experimental techniques *Phys. Med. Biol.* **42** 825–40

Hielscher A H, Alcouffe R E and Barbour R L 1998 Comparison of finite-difference transport and diffusion calculations for photon migration in homogeneous and heterogeneous tissues *Phys. Med. Biol.* **43** 1285–1302

Iftimia N and Jiang H 2000 Quantitative optical image reconstruction of turbid media by use of direct-current measurements *Appl. Opt.* **39** 5256–61

Jiang H 1999 Optical image reconstruction based on the third-order diffusion equations *Opt. Express* **4** 241–6

Jiang H, Paulsen K D, Osterberg U L, Pogue B W and Patterson M S 1996 Optical image reconstruction using frequency-domain data: simulations and experiments *J. Opt. Soc. Am* A **13** 253–66

Jiang H, Xu Y and Iftimia N 2000 Experimental three-dimensional optical image reconstruction of heterogeneous turbid media *Opt. Express* **7** 204–9

Jiang H, Xu Y, Iftimia N, Eggert J, Klove K, Barron L Lisa and Fajardo L 2001 Three-dimensional optical tomographic imaging of breast in a human subject *IEEE Trans. Med. Imag.* **20** 1334–40

Kanmani B and Vasu R 2007 Noise-tolerance analysis for detection and reconstruction of absorbing inhomogeneities with diffuse optical tomography using single- and phase-correlated dual-source schemes *Phys. Med. Biol.* **52** 1409–29

Klose A, Netz U, Beuthan J and Hielscher A H 2002 Optical tomography using the time-independent equation of radiative transfer: Part 1. Forward model *J. Quant. Radiat. Spectrosc. Transfer* **72** 691–713

Klose A D and Larson E W 2006 Light transport in biological tissue based on the simplified spherical harmonics equations *J. Comput. Phys.* **220** 441–70

Kim A and Ishimaru A 1998 Optical diffusion of continuous-wave, pilsed, and density waves in scattering media and comparisons with radiative reansfer *Appl. Opt.* **37** 5313–19

Paulsen K D and Jiang H 1995 Spatially-varying optical property reconstruction using a finite element diffusion equation approximation *Med. Phys.* **22** 691–702

Oak Ridge National Laboratory 1990 *RSIC Computer Code Collection Report*

Rui K, Bal G and Hielscher A H 2007 Transport and diffusion-based optical tomography in small volumes: a comparative study *Appl. Opt.* **46** 6669–79

Song Z, Dong K, Hu X H and Lu J Q 1999 Monte Carlo simulations of converging laser beams propagation in biological materials *Appl. Opt.* **38** 2944–49

Unlu M, Birgul O and Gulsen G 2008 A simulation study of the variability of indocyanine green kinetics and using structural a priori information in dynamic contrast enhanced diffuse optical tomography *Phys. Med. Biol.* **53** 3189–3200

Xu M, Cai W, Lax M and Alfano R 2001 Photon transport forward model for imaging in turbid media *Opt. Lett.* **26** 1066–68

Yodh A and Chance B 1995 Spectroscopy and imaging with diffusing light *Phys. Today* **48** 34–40

Yuan Z and Jiang H 2007a Image reconstruction schemes that combines modified Newton method and efficient initial guess estimate for optical tomography of finger joints *Appl. Opt.* **46** 2757–68

Yuan Z and Jiang H 2007b Three-dimensional finite-element-based photoacoustic tomography: reconstruction algorithm and simulation *Med. Phys.* **34** 538–46

Yuan Z, Zhang Q, Sobel E and Jiang H 2007 3D diffuse optical tomography imaging of osteoarthritis: initial results in finger joints *J. Biomed. Opt.* **12** 034001

Yuan Z, Zhang Q, Sobel E and Jiang H 2008 Tomographic x-ray-guided three-dimensional diffuse optical tomography of osteoarthritis in the finger joints *J. Biomed. Opt.* **13** 044006